Towards a Rigorous Theoretical Analysis and Evaluation of GNN Explanations

Chirag Agarwal
Harvard University
chirag_agarwal@hms.harvard.edu

Marinka Zitnik[*]
Harvard University
marinka@hms.harvard.edu

Himabindu Lakkaraju[*]
Harvard University
hlakkaraju@hbs.edu

Abstract

As Graph Neural Networks (GNNs) are increasingly employed in real-world applications, it becomes critical to ensure that the stakeholders understand the rationale behind their predictions. While several GNN explanation methods have been proposed recently, there has been little to no work on theoretically analyzing the behavior of these methods or systematically evaluating their effectiveness. Here, we introduce the first axiomatic framework for theoretically analyzing, evaluating, and comparing state-of-the-art GNN explanation methods. We outline and formalize the key desirable properties that all GNN explanation methods should satisfy in order to generate *reliable* explanations, namely, *faithfulness*, *stability*, and *fairness*. We leverage these properties to present the first ever theoretical analysis of the effectiveness of state-of-the-art GNN explanation methods. Our analysis establishes upper bounds on all the aforementioned properties for popular GNN explanation methods. We also leverage our framework to empirically evaluate these methods on multiple real-world datasets from diverse domains. Our empirical results demonstrate that some popular GNN explanation methods (e.g., gradient-based methods) perform no better than a random baseline and that methods which leverage the graph structure are more effective than those that solely rely on the node features.

1 Introduction

Graph Neural Networks (GNNs) have emerged as powerful tools for effectively representing graph structured data, such as social, information, chemical, and biological networks. As these models are increasingly being employed in critical applications (*e.g.,* drug repurposing [13, 54], crime forecasting [18]), it becomes essential to ensure that the relevant stakeholders can understand and trust their functionality [50]. Only if the stakeholders have a clear understanding of the behavior of these models, they can evaluate when and how much to rely on these models, and detect potential biases or errors in them. To this end, several approaches have been proposed in recent literature to explain the predictions of GNNs [3, 8, 17, 28, 30, 33, 39, 47, 50]. Based on the techniques they employ, these approaches can be broadly characterized into perturbation-based [30, 39, 50], gradient-based [41, 45], and surrogate model based [17, 47] methods [51].

While several approaches have been proposed to explain the predictions of GNNs, evaluating the quality of the resulting explanations is non-trivial. A meaningful GNN explanation should be both *reliable* (i.e., it should accurately capture the behavior of the underlying GNN model consistently), and *inter-*

---

[*]Equal Contribution

pretable (i.e., it should be concise and easy to understand). While interpretability of GNN explanations is commonly assessed using metrics such as *sparsity* (*e.g.,* , number of important attributes) and user studies [51], there is no single, agreed-upon strategy to evaluate the reliability of GNN explanations. Existing methods employ drastically different and highly specific metrics to evaluate explanation reliability (*e.g.,* varying definitions of accuracy, fidelity etc.). For example, GNNEXPLAINER and PGEXPLAINER construct ground truth explanations for synthetic datasets. If a resulting explanation matches the ground truth explanation, it is considered to be correct. This strategy relies heavily on the availability of ground truth explanations which severely limits the kinds of datasets to which it can be applied. GRAPHLIME, on the other hand, artificially adds noisy node attributes into the data and evaluates if the resulting explanations can filter out these *useless* attributes. This strategy encapsulates a rather limited view of reliability and is only applicable to very specific application scenarios because explanations that filter out useful attributes are still considered as reliable by the above definition.

As can be seen, existing strategies for evaluating explanation reliability are both drastically different and highly context specific, i.e., they focus on evaluating very narrow definitions of reliability and/or cater to very specific application settings, datasets, methods, and explanation types. These limitations emphasize the need for a well-defined, generic, and comprehensive evaluation framework which can be used to evaluate the reliability of all GNN explanation methods. Furthermore, there has not been any prior research on theoretically analyzing the behavior and reliability of GNN explanation methods. Without the existence of such rigorous theoretical and empirical frameworks for evaluating explanation reliability, it would be extremely challenging to systematically compare existing explanation methods and determine which ones to employ in what kinds of applications. Therefore, both the aforementioned aspects are critical to the advancement of the literature on GNN explanation methods.

Present Work. Here, we propose the first axiomatic framework to theoretically analyze, evaluate, and compare state-of-the-art GNN explanation methods. To this end, we first identify the desiderata for a *reliable* GNN explanation. More specifically, we posit that a reliable GNN explanation should *faithfully* mimic the predictions of the underlying GNN model, preserve critical characteristics such as *fairness* of the underlying model, and also exhibit *stability* i.e., small perturbations to an instance should not result in drastically different explanations. We formalize the above desiderata in such a way that the desirable properties of *faithfulness*, *stability*, and *fairness* can be readily computed for any given GNN explanation. We then leverage the aforementioned formalisms to present the first ever theoretical analysis of the reliability of several state-of-the-art GNN explanation methods. Our analysis establishes upper bounds on all the aforementioned properties for various explanation methods. Further, empirical analysis of our theoretical bounds indicate that explanation methods satisfied our theoretical bounds across all properties. We also carry out extensive experiments with multiple real-world datasets from diverse domains to systematically evaluate the reliability of several state-of-the-art GNN explanation methods using our proposed framework. Our results shed light on several critical insights: 1) Surrogate model based explanation methods generate more reliable explanations and, on average across four datasets, are more stable than gradient and perturbation-based methods, 2) Random Edge explanations achieve higher faithfulness than some state-of-the-art explanation methods, 3) Current GNN explanation methods do not produce explanations that are simultaneously faithful, stable, and fair.

2   Related Work

This paper builds upon a wealth of previous research at the intersection of explanation methods, graph neural networks and interpretability for graphs, and systematic evaluation of explanations.

Post-hoc explanations and their analysis. A myriad of techniques have been developed for explaining predictions in a post-hoc manner. These techniques differ in their access to the complex model (*i.e.,* black box vs. access to internals), scope of approximation (*i.e.,* global vs. local), search technique (*i.e.,* perturbation-based vs. gradient-based vs. surrogate model-based), and basic units of explanation (*i.e.,* feature importance vs. rule based). In addition to LIME [36] and SHAP [29], there are several other *model-agnostic local explanation* approaches that explain individual predictions [37, 43, 23, 42, 45, 40, 44]. There has also been recent work on constructing *counterfactual explanations* which capture what changes need to be made to an instance in order to flip its prediction [48, 46, 19, 34, 27, 4, 20, 21, 1], and *global explanations* for summarizing the complete behavior of any given black box by approximating it using interpretable models [24, 5, 22].

Explainability in Graph Neural Networks (GNNs). GNNs specify non-linear deep transformation functions that map graph structures (*i.e.,* nodes, edges or entire graphs) into compact vector embeddings [26]. This is typically achieved through a process that iteratively propagates neural messages along edges of a graph and aggregates them at nodes [10]. A variety of GNN architectures have been proposed in the literature [31, 52, 54], and recent research has focused on on developing GNN explanation methods [3, 8, 17, 28, 30, 33, 39, 47, 50]. Early methods developed graph analogs of *gradient-based methods* from computer vision literature, including gradient heatmaps [41], Grad-CAM [40], and integrated gradients [45]. More recently, *perturbation-based methods* [30, 39, 50] explain GNN predictions by finding small subgraphs that are most influential for the prediction w.r.t. different perturbations of the input graph. To this end, GraphMASK [39] identifies edges in each GNN layer that can be dropped without affecting the final prediction. Similarly, GNNExplainer [50] learns real-valued edge and node attribute masks that select influential subgraphs. Finally, *surrogate model-based methods* fit an interpretable model to local neighborhoods of target nodes such that the model faithfully represents GNN model's behavior in network vicinity of target nodes. For example, GraphLIME [17] uses a feature-wise Hilbert-Schmidt independence criterion lasso (HSIC Lasso) as the surrogate model.

Evaluating explainers. Few works have analysed robustness and other properties of post-hoc explanation techniques [25, 6, 9]. However, due to the relative infancy of GNN explainability as a field, rigorous analyses of GNN explanation methods are very limited; use a variety of qualitative and quantitative metrics for evaluating the correctness of explanations, including accuracy, faithfulness, and sparsity [38, 51]; have been conducted only for specific cases; and theoretical analysis has not yet been attempted. As a result, these analyses are not necessarily generalizable and the issue gets further exacerbated as evaluation of explanation methods on real-world graph datasets is highly non-trivial due to the lack of ground-truth information. Further, qualitative evaluations can be subjective whereas quantitative evaluations are mostly driven by accuracy and do not consider other model properties.

3 Our Framework: Formalizing Desirable Properties

A meaningful GNN explanation should be reliable i.e., it should accurately capture the behavior of the underlying GNN model. As discussed earlier, there are no general frameworks for assessing the reliability of explanations generated by GNN explanation methods. To address this shortcoming, we outline key properties that capture the reliability of a GNN explanation, namely, *faithfulness*, *stability*, and *fairness preservation*. This formalization of explanation reliability is highly critical because it paves the way for establishing a common platform for systematically reasoning about, evaluating, and comparing GNN explanation methods.

Notation: Graphs and GNNs. Let $\mathcal{G} = (\mathcal{V}, \mathcal{E}, \mathbf{X})$ denote an undirected and unweighted graph comprising of a set of nodes $\mathcal{V}$, a set of edges $\mathcal{E}$, and a set of node attribute vectors $\mathbf{X} = \{\mathbf{x}_1, \mathbf{x}_2, \ldots, \mathbf{x}_N\}$ corresponding to nodes in $\mathcal{V}$, where $\mathbf{x}_u \in \mathbb{R}^M$. Let $N = |\mathcal{V}|$ denote the number of nodes in the graph and let $\mathbf{A} \in \mathbb{R}^{N \times N}$ be the adjacency matrix where element $\mathbf{A}_{uv} = 1$ if nodes u and v are connected in $\mathcal{G}$, and $\mathbf{A}_{uv} = 0$ otherwise. We use $\mathcal{N}_u$ to denote the set of immediate neighbors of node u excluding itself. Without loss of generality, we consider node classification and use f to denote a GNN model trained to predict properties (labels) for nodes. The model's softmax prediction for node u is given by $\hat{\mathbf{y}}_u = f(\mathcal{G}_u)$, where $\mathcal{G}_u$ denotes the subgraph associated with node u and $\hat{\mathbf{y}}_u \in [0, 1]^C$. The associated adjacency matrix and node attributes for $\mathcal{G}_u$ are denoted by $\mathbf{A}_u \in \{0, 1\}^{N \times N}$ and $\mathbf{X}_u \in \{\mathbf{x}_i | i \in \mathcal{N}_u\}$, respectively. Also, $\hat{y}_u = \arg\max_c \hat{\mathbf{y}}_u$ is the predicted label, where $\hat{y}_u \in \{0, 1, \ldots, C\}$ and C is the number of labels.

Notation: GNN explanations. We consider an instance-based explanation problem, which is the most actively explored type of explanations in GNN literature. It produces explanations as one or several training instances (*i.e.,* nodes, edges, and/or node attributes) that support the model's predictions. Given a node u, an explanation is denoted as E_u comprising a subset of node attributes and a subset of edges identified by the explainer. In particular, the explanation E_u consists of a discrete node attribute mask $\mathbf{r}_u \in \{0, 1\}^M$ for $v \in \mathcal{N}_u$ and/or a discrete edge mask $\mathbf{R}_u \in \{0, 1\}^{N \times N}$, where 1 indicates that a node attribute/edge is included in the explanation and 0 indicates otherwise. We use to denote $t(E_u, \mathcal{G}_u)$ a function that applies masks in E_u to u's subgraph $\mathcal{G}_u$ as follows: $\mathbf{X}_u = \{\mathbf{x}_i \circ \mathbf{r}_i | i \in \mathcal{N}_u\}$ and $\mathbf{A}_u = \mathbf{R}_u \circ \mathbf{A}_u$. Finally, we use $\hat{y}_u^E = f(t(E_u, \mathcal{G}_u))$ to denote prediction for node u produced f on the masked subgraph.

3.1 Faithfulness

A reliable explanation should *faithfully* capture the behavior of the underlying model. More specifically, it should highlight the key attributes that the underlying model leveraged to make any given prediction, filter out any irrelevant attributes, and/or mimic the predictions of the underlying model. Formally, an explanation E_u corresponding to a node u is faithful if it accurately captures the behavior of the underlying model f in the local region around u. To operationalize this, we first generate the local region around u by constructing a set $\mathcal{K}$ of nodes comprising of node u and its perturbations. These perturbations are generated by rewiring the edges incident on node u with a small probability and/or making infinitesimally small changes to its node attributes. Next, we obtain the model predictions as well as explanation E_u's predictions for node u and all its perturbations. Note that the *explanation's predictions* can be obtained by first using the mapping function t which takes an explanation mask and applies it to any given node and its subgraph (See Notation on GNN explanations above) to generate a new masked subgraph. The resulting subgraph can then be passed as input to the model f to obtain a prediction. Summing up the difference between the model and explanation predictions for all the nodes in $\mathcal{K}$ will provide us with an estimate of how *unfaithful* the explanation E_u is. The smaller this estimate, the more faithful the explanation E_u.

Definition 1 (Faithfulness). *Given a set $\mathcal{K}$ comprising of a node u and its perturbations, an explanation E_u corresponding to node u is said to be faithful if:*

$$\sum_{u' \in \mathcal{K}} ||f(\mathcal{G}_{u'}) - f(t(E_u, \mathcal{G}_{u'}))||_2 \leq \delta, \tag{1}$$

where $\mathcal{G}'_u$ denotes the subgraph associated with node u', and δ is an infinitesimally small constant. Note that the left hand side of Eqn. 1 is a measure of unfaithfulness of the explanation E_u. So, higher values indicate higher degree of unfaithfulness.

3.2 Stability

Another key trait of a reliable explanation is that it should exhibit stability *i.e.,* infinitesimally small perturbations to an instance (which do not affect its model prediction) should not change its explanation drastically. This notion of stability has been well studied in other areas of machine learning (ML) including adversarial ML and the broader explainable ML literature [45]. In the context of GNNs, an explanation E_u corresponding to a node u is considered stable if the explanations corresponding to u (*i.e.,* E_u) and its perturbation u' (denoted by E'_u) are similar. Note that the perturbation u' here is generated in the same way as above by rewiring the edges incident on node u with a small probability and/or making infinitesimally small changes to its node attributes.

Definition 2 (Stability). *Given a node u and its perturbation u', an explanation E_u corresponding to node u is said to be stable if:*

$$\mathcal{D}(E_u, E_{u'}) \leq \delta \tag{2}$$

where $E_{u'}$ is the explanation corresponding to node u', $\mathcal{D}(x, y)$ is a distance metric that computes the distance between two explanations, and δ is an infinitesimally small constant. Also, the left hand side of Eqn. 2 is a measure of instability of the explanation E_u. So, higher values indicate higher degree of instability.

3.3 Fairness Preservation

As GNNs are increasingly being employed in critical applications in domains such as financial lending and criminal justice, it becomes important to ensure that the explanations generated by state-of-the-art GNN explanation methods preserve the fairness properties of the underlying model. More specifically, a reliable explanation should always capture the biases in the underlying model. For instance, if a model is biased against a protected group, then its explanations should reflect that. This will help both model developers and practitioners in recognizing and addressing these prejudices. Analogously, if a model is fair, then its explanations should reflect that. To formalize these intuitions, we consider two notions of fairness, namely, *counterfactual fairness* and *group fairness*.

a) Counterfactual Fairness. An explanation E_u corresponding to node u preserves counterfactual fairness if the explanations corresponding to u (i.e., E_u) and its sensitive attribute perturbation u^s (denoted by E_{u^s}) are similar (dissimilar) if their model predictions are similar (dissimilar). Note that

the sensitive attribute perturbation u^s is generated by flipping/modifying the sensitive attribute s in the node attribute vector of u (denoted by $\mathbf{x}_u$) while keeping everything else constant.

Definition 3 (Counterfactual Fairness). *Given a node u and its sensitive attribute perturbation u_s, an explanation E_u corresponding to node u is said to preserve counterfactual fairness if:*

$$\mathcal{D}\big(E_u, E_{u^s}\big) \propto f(\mathcal{G}_u) - f(\mathcal{G}_{u^s}) \tag{3}$$

where E_{u^s} is the explanation corresponding to node u^s, $\mathcal{G}_u$ and $\mathcal{G}'_u$ denote the subgraph associated with node u and u^s respectively.

b) Group Fairness. The notion of group fairness has been quantified using a variety of metrics in literature such as statistical parity [7], equality of opportunity [15] etc. We focus here on statistical parity which ensures that the probability of a positive outcome is independent of the sensitive attribute value (formal definition below). An explanation E_u for node u preserves group fairness if it accurately captures the statistical parity [15] of the underlying model f in the local region around u. To operationalize this, we first generate the local region around u by constructing a set $\mathcal{K}$ of nodes comprising of the original node u, and its perturbations. Next, we obtain the model predictions as well as explanation E_u's predictions for node u and all its perturbations. The perturbations, the model and explanation predictions are obtained in the same way as Section 3.1. We denote the model predictions and explanation predictions using $\hat{\mathbf{y}}_{\mathcal{K}} = \{\hat{y}_1, \hat{y}_2, \ldots, \hat{y}_{|\mathcal{K}|}\}$ and $\hat{\mathbf{y}}_{\mathcal{K}}^{E_u} = \{\hat{y}_1^{E_u}, \hat{y}_2^{E_u}, \ldots, \hat{y}_{|\mathcal{K}|}^{E_u}\}$ respectively. If the statistical parity estimates computed using the two vectors $\hat{\mathbf{y}}_{\mathcal{K}}$ and $\hat{\mathbf{y}}_{\mathcal{K}}^{E_u}$ are similar, then the explanation E_u is said to preserve group fairness. The statistical parity estimates for $\hat{\mathbf{y}}_{\mathcal{K}}$ can be computed as $\mathrm{SP}(\hat{\mathbf{y}}_{\mathcal{K}}) = |\Pr(\hat{y}_{u'}=1|s=0) - \Pr(\hat{y}_{u'}=1|s=1)|$ where the probabilities are computed over all the nodes in $\mathcal{K}$. The statistical parity estimate for $\hat{\mathbf{y}}_{\mathcal{K}}^{E_u}$ can be computed analogously using explanation E_u's predictions.

Definition 4 (Group Fairness). *Given a set $\mathcal{K}$ comprising of a node u and its perturbations, an explanation E_u corresponding to node u preserves group fairness if:*

$$|\,\mathrm{SP}(\hat{\mathbf{y}}_{\mathcal{K}}) - \mathrm{SP}(\hat{\mathbf{y}}_{\mathcal{K}}^{E_u})\,| \leq \delta, \tag{4}$$

where $\mathrm{SP}(\hat{\mathbf{y}}_{\mathcal{K}})$ and $\hat{\mathbf{y}}_{\mathcal{K}}^{E_u}$ are as defined above. Note, the left hand side term of the inequality in Eqn. 4 is a measure of group fairness mismatch. So, higher values indicate that the explanation is not preserving group fairness.

4 Our Theoretical Analysis

Next we derive theoretical bounds of faithfulness (Sec. 4.1), stability (Sec. 4.2), and fairness (Sec. 4.3) for GNN explanation methods. These bounds need only information about the general message passing form of GNNs [10] and do not make any assumptions about the GNN architecture. As we will show, these bounds apply to all commonly used GNN explainability methods. The proposed bounds can be computed efficiently, which makes them suitable for use in empirical evaluations when one wishes to find out which of several explanation methods produces most reliable explanations.

4.1 Analyzing Faithfulness of GNN Explanation Methods

Here, we derive upper bounds on the unfaithfulness of explanations output by state of the art GNN explanation methods.

Theorem 1. *Given a node u and a set $\mathcal{K}$ of node perturbations, the faithfulness property (Sec. 3.1, Eqn. 1) of its explanation E_u can be bounded as follows:*

$$\sum_{u' \in \mathcal{K}} ||f(\mathcal{G}_{u'}) - f(t(E_u, \mathcal{G}_{u'}))||_2 \leq \gamma\,(1 + |\mathcal{K}|)\,||\Delta||_2, \tag{5}$$

where $f(\mathcal{G}_{u'}) = \hat{\mathbf{y}}_{u'}$ are softmax predictions that use original attributes and $f(t(E_u, \mathcal{G}_{u'})) = \hat{\mathbf{y}}_{u'}^E$ are softmax predictions that use attributes marked important by explanation E_u. Further, γ denotes the product of the Lipschitz constants for GNN's activation function and GNN's weight matrices across all layers in the GNN, and Δ is an explanation method-specific term.

Proof Sketch. We show that faithfulness of an explanation method, which generates node attribute explanations, is bounded by $\gamma_{11}\,(1+|\mathcal{K}|)\,||(\mathbf{1} - \mathbf{r}_u) \circ \mathbf{x}_u||_2$, where γ_{11} is a constant comprising

of the product of the Lipschitz constant for GNN's activation function, weights of the final node classification layer, and self-attention weight of node u across all layers of the GNN. Further, we show that faithfulness of an explanation method, which generates edge-level explanations, is bounded by $\gamma_{12} (1+|\mathcal{K}|) \, ||\Delta_{\mathbf{x}_v}||_2$, where γ_{12} is similar to γ_{11} but uses weights associated with u's immediate neighbors instead of self-attention weight, and $\Delta_{\mathbf{x}_v}$ is the difference between embeddings of u's neighbors where we exclude edges that are not part of the explanation (*i.e.,* unnecessary edges as identified by the explanation). Details are in Appendix B.1.

4.2 Analyzing Stability of GNN Explanation Methods

Next, we take a representative explanation method for each of gradient-based (Gradients [41]), perturbation-based (GraphMASK [39]), and surrogate model-based (GraphLIME [17]) methods and derive upper bounds on the stability of their explanations.

Theorem 2 (Gradients). *Given a non-linear activation function σ that is Lipschitz continuous, the stability property (Sec. 3.2, Eqn. 2) of explanation E_u returned by Gradients method can be bounded as follows:*

$$||\nabla_{\mathbf{x}_{u'}} f - \nabla_{\mathbf{x}_u} f||_p \leq \gamma_3 ||\mathbf{x}_{u'} - \mathbf{x}_u||_p, \tag{6}$$

where γ_3 is a constant, $\mathbf{x}_u$ is u's attribute vector, and $\mathbf{x}_{u'}$ is the perturbed attribute vector.

Proof Sketch. We prove that gradient explanations are Lipschitz using data processing inequalities and the Lipschitz constant (γ_3) is the product of the l_p-norm of the difference in the predictions between the original and perturbed node, the weight of the final classification layer, and the weights associated with node u. Details are in Appendix B.2.1.

Theorem 3 (GraphMASK). *Given concatenated embeddings of node u and v, the stability property (Sec. 3.2, Eqn. 2) of explanation E_u returned by GraphMASK method can be bounded as follows:*

$$||z_{u',v}^l - z_{u,v}^l||_2 \leq \gamma_4^l \, ||\mathbf{q}_{u',v}^l - \mathbf{q}_{u,v}^l||_2, \tag{7}$$

where E_u is an edge mask comprising of $z_{u,v}^l$ indicating whether an edge connecting node u and v in layer l can be dropped or not, $q_{u,v}^l$ is the concatenated embeddings for node u and v at layer l, and γ_4^l denotes the Lipschitz constant which is a product of the weights of the l-th fully-connected layer, and the Lipschitz constants for the layer normalization function and softplus activation function.

Proof Sketch. We prove that an explanation generated by GraphMASK for an edge at layer l is Lipschitz and the Lipschitz constant (γ_4^l) is product of the Lipschitz constants of the layer normalization function and the l_2-norm of the weight matrices of the erasure function. Details are in Appendix B.2.2.

Theorem 4 (GraphLIME). *Given the centered Gram matrices for the original and perturbed node attributes, the stability property (Sec. 3.2, Eqn. 2) of explanation E_u returned by GraphLIME method can be bounded as follows:*

$$||\beta_k' - \beta_k||_F \leq \gamma_2 \, \cdot \, \mathrm{tr}((\frac{1}{\mathbf{e}^T \mathbf{W}^{-1} \mathbf{e}})^{-1} - \mathbf{I}), \tag{8}$$

where E_u is a node mask produced using the attribute importance β_k' and β_k generated by GraphLIME for the perturbed and original node attributes, γ_2 is a constant independent of the added noise, $\mathbf{e}$ is a vector of all ones, and $\mathbf{W}$ is a matrix comprising of the added noise terms.

Proof Sketch. We prove that the stability of GraphLIME is bounded by the trace of the Gram matrix for the output label and of the perturbed Gram matrix due to the noise added in the input graph. We first derive the closed-form of the attribute importance coefficient β and then use it derive the upper bounds for the GraphLIMEs' stability. Details are in Appendix B.2.3.

4.3 Analyzing Fairness of GNN Explanation Methods

Here, we analyze the group fairness (Sec. 4.3.1) and counterfactual fairness (Sec. 4.3.2) properties of state-of-the-art GNN explanation methods and derive their corresponding bounds.

4.3.1 Group Fairness

Below, we provide a bound on how well the explanations output by state-of-the-art GNN explanation methods preserve group fairness. Without loss of generality, we consider a binary sensitive attribute s (*e.g.*, gender $\in$ {male, female}).

Theorem 5. *Given a node u, a sensitive attribute s, and a set $\mathcal{K}$ comprising of node u and its perturbations, the group fairness property (Sec. 3.3, Eqn. 4) of an explanation E_u corresponding to node u can be bounded as follows:*

$$| \operatorname{SP}(\hat{\mathbf{y}}_{\mathcal{K}}) - \operatorname{SP}(\hat{\mathbf{y}}_{\mathcal{K}}^{E_u}) | \leq \sum_{s \in \{0,1\}} |\operatorname{Err}_{D_s}(f(t(E_u, \mathcal{G}_{u'})) - f(\mathcal{G}_{u'}))|, \tag{9}$$

where $\operatorname{SP}(\hat{\mathbf{y}}_{\mathcal{K}})$ and $\operatorname{SP}(\hat{\mathbf{y}}_{\mathcal{K}}^{E_u})$ are statistical parity estimates as defined in Sec. 3.3, D is the joint distribution over the node attributes $\mathbf{x}_{u'}$ in graph $\mathcal{G}_{u'}$ and their respective labels $\mathbf{y}_{u'}$ for all nodes $u' \in \mathcal{K}$, D_s is the conditional distribution of D given a particular value of the sensitive attribute s, and $\operatorname{Err}_D(\cdot) = \mathbb{E}_D[\mathbf{y}_{u'} - f(\mathcal{G}_{u'})]$ is the error of the model f under the joint distribution D.

Proof Sketch. We show that the group fairness of any explanation method is bounded by the sum of the errors $\operatorname{Err}_D(\cdot)$ of model f under distribution D conditioned on different values of its sensitive attribute. For the set of $\mathcal{K}$ nodes, the error is computed by taking the expectation of the difference between their respective true labels, set of model predictions using the original node attributes (*i.e.,* node attributes and incident edges), and their corresponding predictions using the explanation E_u. Details are in Appendix B.3.

4.3.2 Counterfactual Fairness

Analogous to the stability analysis (Sec. 4.2), we now derive the bounds for counterfactual fairness of the corresponding algorithms.

Theorem 6 (Gradients). *Given a non-linear activation function σ that is Lipschitz continuous, the counterfactual fairness property (Sec. 3.3, Eqn. 3) of an explanation E_u returned by Gradients method can be bounded as follows:*

$$||\nabla_{\mathbf{x}_{u^s}} f - \nabla_{\mathbf{x}_u} f||_p \leq \gamma_3, \tag{10}$$

where $\mathbf{x}_u$ is attributes for node u and $\mathbf{x}_{u^s}$ is the generated counterfactual by flipping the sensitive attribute of $\mathbf{x}_u$.

Proof Sketch. The p-norm distance between $\mathbf{x}_{u^s}$ and $\mathbf{x}_u$ is one as all the individual node attributes are the same except the sensitive attribute which is flipped (either from $0 \rightarrow 1$ or $1 \rightarrow 0$). The left term in Eqn. 10 is similar to Eqn. 6 of Theorem 2. Hence, using $||\mathbf{x}_{u'} - \mathbf{x}_u||_p=1$ in Eqn. 6, we obtain the equation in Theorem 6.

Theorem 7 (GraphMASK). *Given concatenated embeddings node u and v, the counterfactual fairness property (Sec. 3.3, Eqn. 3) of an explanation E_u returned by GraphMASK method can be bounded as follows:*

$$||z_{u',v}^l - z_{u,v}^l||_2 \leq \gamma_4^l \, ||\mathbf{q}_{u^s,v}^l - \mathbf{q}_{u,v}^l||_2, \tag{11}$$

where γ_4^l is the same constant as defined in Theorem 3.

Proof Sketch. A counterfactual node u^s is generated by flipping/modifying one sensitive attribute from $\mathbf{x}_u$. The left term in Eqn. 11 is similar to Eqn. 7 of Theorem 3. The term $\mathbf{q}_{u^s}^l$ denotes the counterfactual embedding for node u^s. Note, for the first layer, the right term of Eqn. 11 simplifies to just γ_4^l as the p-norm between the $\mathbf{x}_{u^s}$ and $\mathbf{x}_u$ is one, *i.e.,* $||\mathbf{x}_{u^s} - \mathbf{x}_u||_p=1$.

Theorem 8 (GraphLIME). *Given the centered Gram matrices for the original and counterfactual node attributes, the counterfactual fairness property (Sec. 3.3, Eqn. 3) of an explanation E_u returned by GraphLIME method can be bounded as follows:*

$$||\beta_k^s - \beta_k||_F \leq \gamma_2 \, \cdot \, \operatorname{tr}((\frac{1}{\mathbf{e}^T \bar{\mathbf{W}}^{-1} \mathbf{e}})^{-1} - \mathbf{I}), \tag{12}$$

where E_u is a node mask produced using the attribute importance $\beta_k^{'}$ and β_k^s is the attribute importance generated by GraphLIME for the k-th attribute of node u^s.

Proof Sketch. Let us consider the k-th node attribute a binary sensitive attribute where $s \in \{0, 1\}$. Similar to stability, in counterfactual fairness we obtain a matrix $\mathbf{W}$ where η will be either 1 or -1, *i.e.,* $\eta=1$ when flipping the sensitive attribute from $0 \to 1$, and $\eta=-1$ when flipping from $1 \to 0$. This does not change the positive semidefinite and invertible property of $\mathbf{W}$ as all diagonal elements are still 1 (*i.e.,* invertible) and the off-diagonal elements are exponential which are always positive. We denote this modified matrix as $\bar{\mathbf{W}}$. The proof has a similar structure as Theorem 4.

5 Experiments

We proceed with the empirical evaluation of known GNN explanation methods. We address the following key questions: Q1) Can we empirically verify that theoretical bounds are not violated? Q2) Can we identify commonalities and differences in behaviors of explanation methods? Q3) What is the relationship between faithfulness, stability, and fairness, and how can our findings inform the development of future GNN explanation methods?

Datasets. We use four datasets in our experiments. 1) *German credit graph* [2] has 1,000 nodes representing customers in a German bank, connected based on similarity of their credit applications. The task is to classify clients into good vs. bad credit risks considering clients' gender as the sensitive attribute. 2) *Recidivism graph* [2] has 18,876 nodes representing defendants released on bail that are connected based on similarity of their past criminal records and demographics. The task is to classify defendants into bail (*i.e.,* unlikely to commit a violent crime if released) vs. no bail (*i.e.,* likely to commit a violent crime) considering race information as the protected attribute. 3) *Credit defaulter graph* [2] has 30,000 nodes representing individuals connected based on payment behaviors and demographics. The task is to classify individuals into credit card payment vs. no payment on time considering age as the sensitive attribute. 4) *Ogbn-arxiv* citation graph [16] has 169,343 nodes representing CS arXiv papers linked based on who cites whom patterns. The task is to classify papers into 40 thematic categories. Full results for *German credit graph* are in Appendix.

Evaluation metrics. We quantify how "good" the explanations are using properties from Sec. 3. In particular we calculate unfaithfulness (Eqn. 1) as: $\sum_{u' \in \mathcal{K}} ||f(\mathcal{G}_{u'}) - f(t(E_u, \mathcal{G}_{u'}))||_2$, where the difference is between predictions made using original or masked node attribute/edge masks; instability (Eqn. 2) as: $\mathcal{D}(E_u, E_{u'})$, where $\mathcal{D}$ is normalized l_1 distance between explanations generated for the original or perturbed node u; counterfactual fairness mismatch (Eqn. 3) as: $\mathcal{D}(E_u, E_{u^s})$, where $\mathcal{D}$ is normalized l_1 distance between explanations generated for the original and counterfactual node u; and group fairness mismatch (Eqn. 4) as: $|\text{SP}(\hat{\mathbf{y}}_{\mathcal{K}}) - \text{SP}(\hat{\mathbf{y}}_{\mathcal{K}}^{E_u})|$, SP is statistical parity calculated on the group $\mathcal{K}$ of predictions. For each node in the test set, we compute the above metrics and report their average and standard errors for all explanation methods.

Explanation methods. We empirically test nine explanation methods. These are gradient-based methods: Gradients [41], Integrated Gradients [45]; perturbation-based methods: GNNExplainer [50], PGExplainer [30], GraphMASK [39]; and surrogate models: GraphLIME [17], PGMExplainer [47]. As a control, we consider two methods which produce random explanations: Random Node Attributes (a node attribute mask defined by an M-dimensional Gaussian distributed vector) and Random Edges (an $N \times N$ edge mask drawn from a uniform distribution over u's incident edges).

Implementation details. We follow the established approach of generating explanations [17, 50] and use reference implementations of explanation methods. We select top-p ($p = 25\%$) attributes (node attributes or edges) and use them to generate explanations for all explanation methods. In all experiments we use GraphSAGE [14] as the underlying GNN predictor. Additional details on hyperparameter selection, training of the GNN predictor and explanation methods are in Appendix C.

Q1) Results: Explanation methods satisfy theoretical bounds across all properties. We verified our theoretical bounds on nine explanation methods. Fig. 1 shows empirical values and theoretical bounds for unfaithfulness, indicating that no violations of bounds were detected in our experiments. Further, results indicate that empirically calculated unfaithfulness are lower for explanation methods with smaller theoretical bounds, suggesting a strong correspondence between empirical calculations on a real-world dataset and theoretical bounds. While it is remarkable that theoretical bounds can be derived for such a broad range of explanation methods, we note that the bounds are not tight, yet the gap with empirical calculations remains modest and is an order of magnitude smaller than that provided by the worst case upper bound. Results for stability and fairness are in Appendix Figs. 2-3.
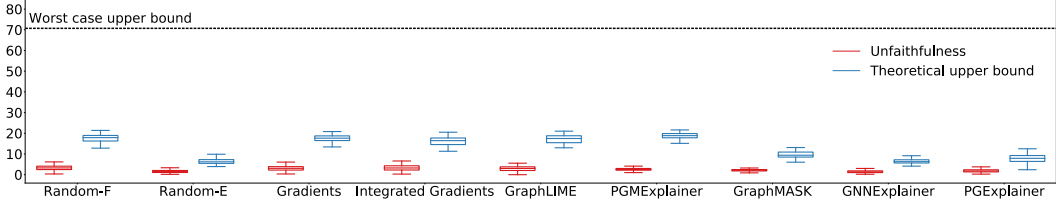
Figure 1: Empirically calculated unfairness (in red) and our theoretical upper bounds for unfaithfulness (in blue) across nine explanation methods. Results on the German credit graph dataset show no violations of the bounds in our experiments. Results for group unfairness and instability are shown in Appendix Figs. 2-3.

Table 1: Systematic evaluation of GNN explanation methods (random strategies (in grey), gradient methods (in yellow), surrogate methods (in purple), and perturbation methods (in red)). Shown are average values of metrics and standard errors across all nodes in the test set. Arrows ($\downarrow$) indicate the direction of better performance. Note that fairness does not apply to the ogbn-arxiv dataset (*i.e.,* N/A) as the dataset does not contain sensitive attributes. See Table 2 for results on all four datasets.

| | | Evaluation metrics | | | |
| | | | | Fairness Mismatch ($\downarrow$) | |
Dataset	Method	Unfaithfulness ($\downarrow$)	Instability ($\downarrow$)	Counterfactual	Group
Recidivism graph	Random Node Attributes	0.312±0.004	0.403±0.002	0.403±0.002	0.144±0.003
	Random Edges	0.040±0.001	0.376±0.000	0.376±0.000	0.046±0.001
	Gradients	0.233±0.004	0.285±0.003	0.173±0.002	0.114±0.002
	Integrated Gradients	0.308±0.005	0.226±0.003	0.104±0.003	0.139±0.003
	GraphLIME	0.191±0.004	0.264±0.004	0.072±0.003	0.107±0.003
	PGMExplainer	0.128±0.001	0.226±0.002	0.223±0.002	0.130±0.002
	GraphMASK	0.053±0.002	0.251±0.003	0.013±0.000	0.060±0.002
	GNNExplainer	0.042±0.001	0.374±0.000	0.364±0.001	0.051±0.002
	PGExplainer	0.056±0.001	0.371±0.001	0.355±0.002	0.064±0.002
Credit defaulter graph	Random Node Attributes	0.098±0.002	0.426±0.002	0.424±0.002	0.045±0.002
	Random Edges	0.020±0.001	0.376±0.000	0.376±0.000	0.017±0.001
	Gradients	0.092±0.002	0.333±0.002	0.171±0.002	0.042±0.002
	Integrated Gradients	0.147±0.003	0.140±0.002	0.069±0.001	0.053±0.002
	GraphLIME	0.038±0.002	0.225±0.004	0.063±0.003	0.018±0.001
	PGMExplainer	0.283±0.002	0.156±0.002	0.154±0.002	0.161±0.003
	GraphMASK	0.012±0.001	0.036±0.002	0.004±0.000	0.010±0.001
	GNNExplainer	0.021±0.001	0.375±0.000	0.366±0.000	0.019±0.001
	PGExplainer	0.028±0.001	0.364±0.001	0.348±0.002	0.022±0.001
Ogbn-arxiv	Random Node Attributes	0.529±0.002	0.375±0.000	N/A	N/A
	Random Edges	0.431±0.002	0.378±0.001	N/A	N/A
	Gradients	0.528±0.002	0.359±0.001	N/A	N/A
	Integrated Gradients	0.528±0.002	0.372±0.000	N/A	N/A
	GraphLIME	0.260±0.003	0.374±0.004	N/A	N/A
	PGMExplainer	0.413±0.002	0.270±0.002	N/A	N/A
	GraphMASK	0.586±0.001	0.125±0.002	N/A	N/A
	GNNExplainer	0.430±0.001	0.376±0.001	N/A	N/A
	PGExplainer	0.338±0.002	0.381±0.001	N/A	N/A

Q2) Results: Surrogate model based methods generate most reliable explanations. Results in Table 1 show that surrogate model based explanation methods tend to produce more reliable explanations than gradient and perturbation based methods. We observe that while all explanation methods do not simultaneously preserve all properties, surrogate methods outperform other methods in stability (+39.6%) and group fairness (+54%), whereas perturbation-based methods outperform other methods in faithfulness (+287%) and counterfactual fairness (+178.8%). Interestingly, we find that the Random Edges approach, forming explanations by random sets of edges found in the vicinity of target nodes, achieves the best faithfulness on German credit and Recidivism graphs, outperforming state-of-the-art explanation methods. Further, the Random Edges approach is among top-performing methods on Credit defaulter and Ogbn-arxiv graphs, highlighting the urgent need for rigorous evaluation and analysis of GNN explainers.

Q3) Results: Trade-offs between faithfulness, stability, and fairness. Our analyses yield similar results across datasets and families of explanation methods (Table 1). In particular, we find that none of the current explanation methods can consistently produce explanations that are simultaneously faithful, stable, and fair. State-of-the-art explanation methods are optimized to prioritize faithfulness over stable and fair explanations, suggesting that GNN explanation methods do not generate reliable explanations and that there are ample opportunities for algorithmic innovation.

6 Conclusions and Future Work

We have developed an axiomatic framework to theoretically analyze, empirically evaluate, and compare GNN explanation methods. The framework identifies the axes of faithfulness, stability, and fairness that, when taken together, can characterize the reliability of any GNN explanation. Further, it establishes theoretical upper bounds on the reliability of explanations for all known GNN explanation methods. Empirical study of nine explanation methods showed that surrogate model based explanation methods generally produce the most reliable explanations across all datasets. Moving forward, it would be interesting to consider other types of explanations, such as counterexamples and global explanations, as they become available in the literature.

References

[1] Chirag Agarwal and Anh Nguyen. Explaining image classifiers by removing input features using generative models. In *ACCV*, 2020.

[2] Chirag Agarwal, Himabindu Lakkaraju, and Marinka Zitnik. Towards a unified framework for fair and stable graph representation learning. In *UAI*, 2021.

[3] Federico Baldassarre and Hossein Azizpour. Explainability techniques for graph convolutional networks. In *ICML Workshop on Learning and Reasoning with Graph-Structured Data*, 2019.

[4] Solon Barocas, Andrew Selbst, and Manish Raghavan. The hidden assumptions behind counterfactual explanations and principal reasons. In *ACM Conference on Fairness, Accountability, and Transparency*, pages 80–89, 2020.

[5] Osbert Bastani, Carolyn Kim, and Hamsa Bastani. Interpretability via model extraction. *CoRR, abs/1706.09773*, 2017.

[6] Prasad Chalasani, Jiefeng Chen, Amrita Roy Chowdhury, Xi Wu, and Somesh Jha. Concise explanations of neural networks using adversarial training. In *International Conference on Machine Learning*, pages 1383–1391, 2020.

[7] Cynthia Dwork, Moritz Hardt, Toniann Pitassi, Omer Reingold, and Richard Zemel. Fairness through awareness. In *Innovations in Theoretical Computer Science Conference (ITSC)*, pages 214–226. ACM, 2012.

[8] Lukas Faber, Amin K Moghaddam, and Roger Wattenhofer. Contrastive graph neural network explanation. In *ICML Workshop on Graph Representation Learning and Beyond*, 2020.

[9] Damien Garreau and Ulrike von Luxburg. Looking deeper into LIME. *CoRR*, abs/2008.11092, 2020.

[10] Justin Gilmer, Samuel S Schoenholz, Patrick F Riley, Oriol Vinyals, and George E Dahl. Neural message passing for quantum chemistry. In *ICML*, pages 1263–1272. PMLR, 2017.

[11] Henry Gouk, Eibe Frank, Bernhard Pfahringer, and Michael J Cree. Regularisation of neural networks by enforcing lipschitz continuity. In *Machine Learning*. Springer, 2021.

[12] Arthur Gretton, Olivier Bousquet, Alex Smola, and Bernhard Schölkopf. Measuring statistical dependence with hilbert-schmidt norms. In *ICALT*, 2005.

[13] Deisy Morselli Gysi, Ítalo Do Valle, Marinka Zitnik, Asher Ameli, Xiao Gan, Onur Varol, Helia Sanchez, Rebecca Marlene Baron, Dina Ghiassian, Joseph Loscalzo, et al. Network medicine framework for identifying drug repurposing opportunities for COVID-19. *arXiv*, 2020.

[14] William L Hamilton, Rex Ying, and Jure Leskovec. Inductive representation learning on large graphs. In *NeurIPS*, 2017.

[15] Moritz Hardt, Eric Price, and Nathan Srebro. Equality of opportunity in supervised learning. In *Neural Information Processing Systems (NIPS)*, 2016.

[16] Weihua Hu, Matthias Fey, Marinka Zitnik, Yuxiao Dong, Hongyu Ren, Bowen Liu, Michele Catasta, and Jure Leskovec. Open graph benchmark: Datasets for machine learning on graphs. In *NeurIPS*, 2020.

[17] Qiang Huang, Makoto Yamada, Yuan Tian, Dinesh Singh, Dawei Yin, and Yi Chang. Graphlime: Local interpretable model explanations for graph neural networks. *arXiv*, 2020.

[18] Guangyin Jin, Qi Wang, Cunchao Zhu, Yanghe Feng, Jincai Huang, and Jiangping Zhou. Addressing crime situation forecasting task with temporal graph convolutional neural network approach. In *ICMTMA*. IEEE, 2020.

[19] Amir-Hossein Karimi, Gilles Barthe, Borja Balle, and Isabel Valera. Model-agnostic counterfactual explanations for consequential decisions, 2019.

[20] Amir-Hossein Karimi, Bernhard Schölkopf, and Isabel Valera. Algorithmic recourse: from counterfactual explanations to interventions. *CoRR, abs/2002.06278*, 2020.

[21] Amir-Hossein Karimi, Julius von Kügelgen, Bernhard Schölkopf, and Isabel Valera. Algorithmic recourse under imperfect causal knowledge: a probabilistic approach. *CoRR, abs/2006.06831*, 2020.

[22] Been Kim, Martin Wattenberg, Justin Gilmer, Carrie J. Cai, James Wexler, Fernanda B. Viégas, and Rory Sayres. Interpretability beyond feature attribution: Quantitative testing with concept activation vectors (TCAV). In *International Conference on Machine Learning*, 2018.

[23] Pang Wei Koh and Percy Liang. Understanding black-box predictions via influence functions. In *International Conference on Machine Learning*, pages 1885–1894, 2017.

[24] Himabindu Lakkaraju, Ece Kamar, Rich Caruana, and Jure Leskovec. Faithful and customizable explanations of black box models. In *AAAI Conference on Artificial Intelligence, Ethics, and Society*, 2019.

[25] Alexander Levine, Sahil Singla, and Soheil Feizi. Certifiably robust interpretation in deep learning. *CoRR, abs/1905.12105*, 2019.

[26] Michelle M Li, Kexin Huang, and Marinka Zitnik. Representation learning for networks in biology and medicine: Advancements, challenges, and opportunities. *arXiv:2104.04883*, 2021.

[27] Arnaud Looveren and Janis Klaise. Interpretable counterfactual explanations guided by prototypes. *CoRR, abs/ 1907.02584*, 2019.

[28] Ana Lucic, Maartje ter Hoeve, Gabriele Tolomei, Maarten de Rijke, and Fabrizio Silvestri. Cf-gnnexplainer: Counterfactual explanations for graph neural networks. *arXiv*, 2021.

[29] Scott M Lundberg and Su-In Lee. A unified approach to interpreting model predictions. In *Advances in Neural Information Processing Systems*, pages 4765–4774, 2017.

[30] Dongsheng Luo, Wei Cheng, Dongkuan Xu, Wenchao Yu, Bo Zong, Haifeng Chen, and Xiang Zhang. Parameterized explainer for graph neural network. In *NeurIPS*, 2020.

[31] Aldo Pareja, Giacomo Domeniconi, Jie Chen, Tengfei Ma, Toyotaro Suzumura, Hiroki Kanezashi, Tim Kaler, Tao Schardl, and Charles Leiserson. EvolveGCN: Evolving graph convolutional networks for dynamic graphs. In *AAAI*, volume 34, pages 5363–5370, 2020.

[32] Hanchuan Peng and Chris Ding. Minimum redundancy and maximum relevance feature selection and recent advances in cancer classification. In *Feature Selection for Data Mining*, 2005.

[33] Phillip E Pope, Soheil Kolouri, Mohammad Rostami, Charles E Martin, and Heiko Hoffmann. Explainability methods for graph convolutional neural networks. In *CVPR*, 2019.

[34] Rafael Poyiadzi, Kacper Sokol, Raul Santos-Rodriguez, Tijl De Bie, and Peter Flach. FACE: Feasible and actionable counterfactual explanations. In *AAAI/ACM Conference on AI, Ethics, and Society*, page 344–350, 2020.

[35] Robert Reams. Hadamard inverses, square roots and products of almost semidefinite matrices. In *Linear Algebra and its Applications*, 1999.

[36] Marco Tulio Ribeiro, Sameer Singh, and Carlos Guestrin. "Why should I trust you?" Explaining the predictions of any classifier. In *ACM SIGKDD International Conference on Knowledge Discovery and Data Mining*, pages 1135–1144, 2016.

[37] Marco Tulio Ribeiro, Sameer Singh, and Carlos Guestrin. Anchors: High-precision model-agnostic explanations. In *AAAI Conference on Artificial Intelligence*, 2018.

[38] Benjamin Sanchez-Lengeling, Jennifer Wei, Brian Lee, Emily Reif, Peter Wang, Wesley Wei Qian, Kevin McCloskey, Lucy Colwell, and Alexander Wiltschko. Evaluating attribution for graph neural networks. In *NeurIPS*, 2020.

[39] Michael Sejr Schlichtkrull, Nicola De Cao, and Ivan Titov. Interpreting graph neural networks for nlp with differentiable edge masking. In *ICLR*, 2021.

[40] Ramprasaath R Selvaraju, Michael Cogswell, Abhishek Das, Ramakrishna Vedantam, Devi Parikh, and Dhruv Batra. Grad-cam: Visual explanations from deep networks via gradient-based localization. In *ICCV*, 2017.

[41] Karen Simonyan, Andrea Vedaldi, and Andrew Zisserman. Deep inside convolutional networks: Visualising image classification models and saliency maps. In *Workshop at ICLR*, 2014.

[42] Karen Simonyan, Andrea Vedaldi, and Andrew Zisserman. Deep inside convolutional networks: Visualising image classification models and saliency maps. In *International Conference on Learning Representations*, 2014.

[43] Dylan Slack, Sophie Hilgard, Sameer Singh, and Himabindu Lakkaraju. How much should I trust you? modeling uncertainty of black box explanations. *CoRR, abs/2008.05030*, 2020.

[44] Daniel Smilkov, Nikhil Thorat, Been Kim, Fernanda Viégas, and Martin Wattenberg. Smooth-grad: Removing noise by adding noise. *CoRR*, abs/1706.03825, 2017.

[45] Mukund Sundararajan, Ankur Taly, and Qiqi Yan. Axiomatic attribution for deep networks. In *ICML*. PMLR, 2017.

[46] Berk Ustun, Alexander Spangher, and Yang Liu. Actionable recourse in linear classification. In *ACM Conference on Fairness, Accountability, and Transparency*, pages 10–19, 2019.

[47] Minh N Vu and My T Thai. Pgm-explainer: Probabilistic graphical model explanations for graph neural networks. In *NeurIPS*, 2020.

[48] Sandra Wachter, Brent Mittelstadt, and Chris Russell. Counterfactual explanations without opening the black box: Automated decisions and the GDPR. *Harvard Journal of Law & Technology*, 31:841, 2017.

[49] Makoto Yamada, Wittawat Jitkrittum, Leonid Sigal, Eric P Xing, and Masashi Sugiyama. High-dimensional feature selection by feature-wise kernelized lasso. In *Neural computation*, 2014.

[50] Rex Ying, Dylan Bourgeois, Jiaxuan You, Marinka Zitnik, and Jure Leskovec. Gnnexplainer: Generating explanations for graph neural networks. In *NeurIPS*, 2019.

[51] Hao Yuan, Haiyang Yu, Shurui Gui, and Shuiwang Ji. Explainability in graph neural networks: A taxonomic survey. *arXiv*, 2020.

[52] Seongjun Yun, Minbyul Jeong, Raehyun Kim, Jaewoo Kang, and Hyunwoo J Kim. Graph transformer networks. *NeurIPS*, 2019.

[53] Han Zhao and Geoffrey J Gordon. Inherent tradeoffs in learning fair representations. In *NeurIPS*, 2019.

[54] Marinka Zitnik, Monica Agrawal, and Jure Leskovec. Modeling polypharmacy side effects with graph convolutional networks. In *Bioinformatics*, 2018.

A   Broad Range of GNN Explanation Methods

We now provide an in-depth overview of the different GNN explanation methods that we analyze in this work. As described in the main text, a graph $\mathcal{G} = (\mathcal{V}, \mathcal{E}, \mathbf{X})$ denote an undirected and unweighted graph comprising of a set of nodes $\mathcal{V}$, a set of edges $\mathcal{E}$, and a set of node attribute vectors $\mathbf{X} = \{\mathbf{x}_1, \mathbf{x}_2, \ldots, \mathbf{x}_N\}$ corresponding to nodes in $\mathcal{V}$, where $\mathbf{x}_u \in \mathbb{R}^M$. The GNN model's f softmax prediction for node u is given by $\hat{\mathbf{y}}_u = f(\mathcal{G}_u)$, where $\mathcal{G}_u$ denotes the subgraph associated with node u and $\hat{\mathbf{y}}_u \in [0, 1]^C$. The associated adjacency matrix and node attributes for $\mathcal{G}_u$. Finally, the explanation E_u consists of a discrete node attribute mask $\mathbf{r}_u \in \{0, 1\}^M$ for $v \in \mathcal{N}_u$ and/or a discrete edge mask $\mathbf{R}_u \in \{0, 1\}^{N \times N}$, where 1 indicates that a node attribute/edge is included in the explanation and 0 indicates otherwise.

Random Explanations. As a control, we consider two methods which produce random explanations: 1) *Random Node Attributes*–a node attribute mask defined by an M-dimensional Gaussian distributed vector; and 2) *Random Edges*–an $N \times N$ edge mask drawn from a uniform distribution over u's incident edges.

GNN Gradients. Gradient [41] based explanation generate local explanations for the prediction of a differentiable GNN model f using its gradient with respect to the node features $\mathbf{x}_u$: $\nabla_{\mathbf{x}_u} f$. Intuitively, gradient represents how much difference a tiny change in each feature of a node u would make to its corresponding classification score. GNN Gradients output an M-dimensional vector that comprises the vanilla gradient of the model, as explanations.

Integrated Gradients. Gradient explanations are often noisy and suffer from saturation problems [45]. Integrated gradients addresses the gradient saturation problem by averaging the gradients over a set of interpolated inputs derived using node u's attribute and a baseline. Formally, integrated gradient explanation for a node u is an M-dimensional vector given by:

$$E_u = (\mathbf{x}_u - \tilde{\mathbf{x}}) \times \int_{\alpha=0}^{1} \frac{\partial f(\mathcal{G}_{u'})}{\partial \mathbf{x}_u} d\alpha, \tag{13}$$

where $\tilde{\mathbf{x}}$ is the baseline input which can be vector of all zeros/ones and $\mathcal{G}_{u'}$ denotes the graph with the interpolated node attribute $\mathbf{x}_{u'} = \tilde{\mathbf{x}} + \alpha(\mathbf{x}_u - \tilde{\mathbf{x}})$.

GraphLIME. GraphLIME [17] is a local interpretable model explanation for GNNs that identifies a nonlinear interpretable model over the neighbors of a node that is locally faithful to the node's prediction. It considers a feature-wise kernelized nonlinear method called Hilbert-Schmidt Independence Criterion Lasso (HSIC Lasso) as an explanation model. For each node prediction, the HSIC Lasso objective function is defined as:

$$\min_{\beta \in \mathbb{R}^d} \frac{1}{2} ||\mathbf{L} - \sum_{k=1}^{M} \beta_k \mathbf{K}^{(k)}||_F^2 + \rho ||\beta||_1, \tag{14}$$

where $|| \cdot ||_F$ is the Frobenius norm, $\rho \geq 0$ is the regularization parameter, $|| \cdot ||_1$ is the l_1 norm to enforce sparsity, $\mathbf{L}$ is the centered Gram matrix, $L_{ij} = L(y_i, y_j)$ is the kernel for the output labels of the nodes, $\mathbf{K}^k$ is the centered gram matrix for the k-th feature, and $K_{ij} = K(x_i^{(k)}, x_j^{(k)})$ is the kernel for the k-th dimensional input node features $\mathbf{x}_u$.

PGMExplainer. Probabilistic Graphical models (PGMs) are statistical models that encode complex distributions using graph-based representation and provides a simple interpretation of the dependencies of those underlying random variables. Specifically, Bayesian network, a PGM represents conditional dependencies among variables via a directed acyclic graph. Given a target prediction $\hat{y}_u$ to be explained, our proposed PGM explanation is the optimal Bayesian network $\mathcal{B}^*$ of the following optimization:

$$\underset{\mathcal{B} \in \mathcal{B}_{E_u}}{\arg\max} \, R_{\hat{y}_u}(\mathcal{B}), \tag{15}$$

where $R_{\hat{y}_u} : E_u \rightarrow \mathbb{R}$ associates each explanation with a score, $\mathcal{B}_{E_u}$ is the set of all Bayesian networks, the optimization is subjected to the condition that the number of variables in $\mathcal{B}$ is bounded by a constant to encourage a compact solution and another constraint to ensure that the target prediction is included in the explanation.

GraphMASK. GraphMASK [39] detect edges at each layer l that can be ignored without affecting the output model predictions. In general, dropping edges from a given graph is non-trivial, and, hence,

for each edge at layer l, GraphMASK learns a binary choice $z_{u,v}^l$ that indicates whether the edge can be dropped, and then replaces the given edge with a learned baseline. Here, $z_{u,v}^l$ indicates an edge connecting node u and v. GraphMASK learns $z_{u,v}^l$ for all $(u,v) \in \mathcal{E}$ for the training data points using an erasure function g_π, where π denotes the parameters of g. For explaining a given prediction, GraphMASK uses this trained function g_π and generates a masked representation of the graph using:

$$\tilde{h}_u^l = \mathbf{Z}^l \circ h_u^l + \alpha^l \circ (1 - \mathbf{Z}^l), \tag{16}$$

where $\mathbf{Z}^l$ comprises of all the individual binary scores $z_{u,v}^l = g_\pi(h_u^l, h_v^l)$, α^l is the learned baseline, and '$\circ$' denotes the element-wise Hadamard product.

GNNExplainer. For a single-instance explanation for node u, GNNExplainer [50] generates an explanation by identifying a subgraph of the computation graph for u and a subset of node features that are most influential for the model f's prediction. Formally, GNNExplainer determines the importance of individual node attributes and incident edges for node u by leveraging Mutual Information (MI) using the following optimization framework:

$$\max_{\mathcal{G}_S} MI(Y, (\mathcal{G}_S, \mathbf{X}_S)), \tag{17}$$

where $\mathcal{G}_S \subseteq \mathcal{G}_u$ is a subgraph and $\mathbf{X}_S$ is the associated node attributes that are important for the GNN's prediction $\hat{y}_u$. Intuitively, MI quantifies the change in probability of prediction $\hat{y}_u$ when u's computation graph is limited to the explanation graph $\mathcal{G}_S$ and its corresponding node attributes $\mathbf{X}_S$.

PGExplainer. In contrast to GNNExplainer, PGExplainer [30] generates explanation only on the graph structure. The direct optimization of the mutual information framework in Eqn. 17 is intractable [50, 30]. Thus, PGExplainer consider a relaxation by assuming that the explanatory graph $\mathcal{G}_S$ is a Gilbert random graph, where selections of edges from the input graph $\mathcal{G}_u$ are conditionally independent to each other. Due to the discrete nature of $\mathcal{G}_S$, PGExplainer employs the *reparameterization trick* where they relax the edge weights from binary to continuous variables in the range $(0, 1)$ and then optimize the objective function using gradient-based methods. It approximates the sampling process of $\mathcal{G}_S$ with a determinant function of parameters Ω, temperature ρ, and an independent random variable ϵ. Specifically, the weight for each edge $\hat{e}(i, j)$ is calculated by:

$$\epsilon \sim \text{Uniform}(0,1), \quad \hat{e}(i,j) = \sigma((\log\epsilon - \log(1-\epsilon) + \omega_{ij})/\rho), \tag{18}$$

where $\sigma(\cdot)$ is the Sigmoid function, $\omega_{ij} \in \mathbb{R}$ is a trainable parameter. With the reparameterization, the objective function of PGExplainer becomes:

$$\min_{\Omega} \mathbb{E}_{\epsilon \sim \text{Uniform}(0,1)} H(Y|\mathcal{G}_u = \hat{\mathcal{G}}_S), \tag{19}$$

where H is the conditional entropy when the computational graph for $\mathcal{G}_u$ is restricted to $\mathcal{G}_S$.

B Proofs for Theorems in Section 4

B.1 Analyzing Faithfulness of GNN Explanation Methods

Theorem 1. *Given a node u and a set of $\mathcal{K}$ of node perturbations, the faithfulness property (Sec. 3.1, Eqn. 1) of its explanation E_u can be bounded as follows:*

$$\sum_{u' \in \mathcal{K}} ||f(\mathcal{G}_{u'}) - f(t(E_u, \mathcal{G}_{u'}))||_2 \leq \gamma \, (1 + |\mathcal{K}|) \, ||\Delta||_2, \tag{20}$$

where $f(\mathcal{G}_{u'}) = \hat{\mathbf{y}}_{u'}$ and $f(t(E_u, \mathcal{G}_{u'})) = \hat{\mathbf{y}}_{u'}^E$ are the softmax predictions using the original attributes and the attributes marked important by the explanation E_u for the original and perturbed nodes respectively, γ is a product of the Lipschitz constants of the activation function and the weight matrices of all message-passing layers in the GNN model, and Δ term is dependent on the explanations provided by the explainer method.

Proof. Without loss of generality, we use a two-layer GNN model for our proof and show its extension to a GNN model with L layers. The two-layer GNN formulated as a message-passing network is defined as:

$$\mathbf{h}_u^1 = \text{sp}(\mathbf{W}_a^1 \mathbf{x}_u + \mathbf{W}_n^1 \sum_{v \in \mathcal{N}_u} \mathbf{x}_v)$$

$$\mathbf{h}_u^2 = \mathbf{W}_{\text{fc}} \mathbf{h}_u^1 + \mathbf{b}$$

$$\hat{\mathbf{y}}_u = \text{softmax}(\mathbf{h}_u^2),$$

where $\mathbf{W}_n^1$ is the weight matrix associated with the neighbors of node u, $\mathbf{W}_a^1$ is the self-attention weight matrix at layer one, and "sp" is the softplus activation function. For the fully-connected layer, we have $\mathbf{W}_{\text{fc}}$ as the weight matrix and $\mathbf{b}$ as the bias term. The softplus function is a smooth approximation of the ReLU function. We generate $|\mathcal{K}|$ perturbations of node u by adding normal Gaussian noise to the node features, *i.e.,* $\mathbf{x}_{u'} = \mathbf{x}_u + \tau$, and rewire edges with some probability p_r. For faithfulness, we get the predictions for node u using the weighted node features of node u, *i.e.,* the element-wise product between $\mathbf{r}_u$ (the feature importance mask generated as an explanation) and $\mathbf{x}_u$. Let $\hat{\mathbf{y}}_u^E$ denote the softmax output for node u using the explanation E_u, *i.e.,* $f(t(E_u, \mathcal{G}_u))$. Therefore, the updated equations using the explanations are:

$$(\mathbf{h}_u^1)^E = \text{sp}\big(\mathbf{W}_a^1(\mathbf{r}_u \circ \mathbf{x}_u) + \mathbf{W}_n^1 \sum_{v \in \mathcal{N}_u'} \mathbf{x}_v\big)$$

$$(\mathbf{h}_u^2)^E = \mathbf{W}_{\text{fc}}(\mathbf{h}_u^1)^E + \mathbf{b}$$

$$\hat{\mathbf{y}}_u^E = \text{softmax}((\mathbf{h}_u^2)^E),$$

where $\mathcal{N}_u'$ denotes the new neighborhood for node u due to the adjacency mask matrix $\mathbf{R}_u$. The difference between the predicted labels for the original and the important node features can be given as:

$$\hat{\mathbf{y}}_u - \hat{\mathbf{y}}_u^E = \text{softmax}(\mathbf{h}_u^2) - \text{softmax}((\mathbf{h}_u^2)^E) \tag{21}$$

Corollary 1. *For any differentiable function* $g : \mathbb{R}^a \to \mathbb{R}^b$,

$$||g(x) - g(y)||_2 \leq ||\mathbf{J}||_F^* ||x - y||_2 \quad \forall x, y \in \mathbb{R}, \tag{22}$$

where $||\mathbf{J}||_F^* = \max_x ||\mathbf{J}||_F$ and $\mathbf{J}$ is the Jacobian matrix of $g(x)$ w.r.t. x. This is implied from the mean value theorem, where for any function $g(x)$ and its derivative $\frac{\partial g(x)}{\partial x}$, we have: $g(x) - g(y) = \frac{\partial g(\phi)}{\partial \phi}(x - y)$, for some $\phi \in (y, x)$.

Hence, taking the norm on both sides in Eqn. 21, we get,

$$||\hat{\mathbf{y}}_u - \hat{\mathbf{y}}_u^E||_2 = ||\text{softmax}(\mathbf{h}_u^2) - \text{softmax}((\mathbf{h}_u^2)^E)||_2$$

$$\leq \mathcal{C}_{\text{fc}} ||\mathbf{h}_u^2 - (\mathbf{h}_u^2)^E||_2, \qquad \text{(Using Corollary 1)}$$

where $\mathcal{C}_{\text{fc}}$ represents the Lipschitz constant for the softmax function. Substituting the values of $\mathbf{h}_u^2$ and $(\mathbf{h}_u^2)^E$ we get:

$$||\hat{\mathbf{y}}_u - \hat{\mathbf{y}}_u^E||_2 \leq \mathcal{C}_{\text{fc}} ||\mathbf{W}_{\text{fc}} \mathbf{h}_u^1 + \mathbf{b} - \mathbf{W}_{\text{fc}}(\mathbf{h}_u^1)^E - \mathbf{b}||_2$$

$$\leq \mathcal{C}_{\text{fc}} ||\mathbf{W}_{\text{fc}} \mathbf{h}_u^1 - \mathbf{W}_{\text{fc}}(\mathbf{h}_u^1)^E||_2$$

$$\leq \mathcal{C}_{\text{fc}} ||\mathbf{W}_{\text{fc}}||_2 ||\mathbf{h}_u^1 - (\mathbf{h}_u^1)^E||_2 \qquad \text{(Using Cauchy-Schwartz inequality)}$$

Substituting the values of $\mathbf{h}_u^1$ and $(\mathbf{h}_u^1)^E$ we get:

$$||\hat{\mathbf{y}}_u - \hat{\mathbf{y}}_u^E||_2 \leq \mathcal{C}_{\text{fc}} ||\mathbf{W}_{\text{fc}}||_2 ||\text{sp}\big(\mathbf{W}_a^1 \mathbf{x}_u + \mathbf{W}_n^1 \sum_{v \in \mathcal{N}_u} \mathbf{x}_v\big) - \text{sp}\big(\mathbf{W}_a^1(\mathbf{r}_u \circ \mathbf{x}_u) + \mathbf{W}_n^1 \sum_{v \in \mathcal{N}_u'} \mathbf{x}_v\big)||_2$$

$$\leq \mathcal{C}_{\text{fc}} \, \mathcal{C}_1 \, ||\mathbf{W}_{\text{fc}}||_2 ||\mathbf{W}_a^1 \mathbf{x}_u + \mathbf{W}_n^1 \sum_{v \in \mathcal{N}_u} \mathbf{x}_v - \mathbf{W}_a^1(\mathbf{r}_u \circ \mathbf{x}_u) - \mathbf{W}_n^1 \sum_{v \in \mathcal{N}_u'} \mathbf{x}_v||_2$$

$$\text{(Using Corollary 1)}$$

$$\leq \mathcal{C}_{\text{fc}} \, \mathcal{C}_1 \, ||\mathbf{W}_{\text{fc}}||_2 \big(||\mathbf{W}_a^1\big(\mathbf{x}_u - (\mathbf{r}_u \circ \mathbf{x}_u)\big)||_2 + ||\mathbf{W}_n^1 \Delta_{\mathbf{x}_v}||_2\big), \qquad \text{(Using triangle inequality)}$$

where $\Delta_{\mathbf{x}_v}$ is the difference between the representations of the neighbors of u after dropping edges using the edge masks. This difference can be neglected for gradient and GraphLIME methods as they provide explanations in the node feature space. Now, using Cauchy-Schwartz inequality, the prediction difference for a node u using its original and just important node features is bounded by:

$$||\hat{\mathbf{y}}_u - \hat{\mathbf{y}}_u^E||_2 \leq \mathcal{C}_{\text{fc}} \, \mathcal{C}_1 \, ||\mathbf{W}_{\text{fc}}||_2 \, ||\mathbf{W}_a^1||_2 \, ||(\mathbf{1} - \mathbf{r}_u) \circ \mathbf{x}_u)||_2, \tag{23}$$

where $\mathcal{C}_1$ is the Lipschitz constant for the softplus activation function and $\mathbf{1} \in \mathbb{R}^M$ is vector with all ones. For mathematical brevity, let $\gamma_{11} = \mathcal{C}_{\text{fc}} \, \mathcal{C}_1 \, ||\mathbf{W}_{\text{fc}}||_2 \, ||\mathbf{W}_a^1||_2$. Similarly, the prediction difference for GraphMASK which provides an explanation with respect to edges is bounded by:

$$||\hat{\mathbf{y}}_u - \hat{\mathbf{y}}_u^E||_2 \leq \mathcal{C}_{\text{fc}} \, \mathcal{C}_1 \, ||\mathbf{W}_{\text{fc}}||_2 \, ||\mathbf{W}_n^1||_2 \, ||\Delta_{\mathbf{x}_v}||_2, \tag{24}$$

where $\gamma_{12} = \mathcal{C}_{\text{fc}} \, \mathcal{C}_1 \, ||\mathbf{W}_{\text{fc}}||_2 \, ||\mathbf{W}_n^1||_2$.

Node feature explanations. Since all the perturbed nodes use the same node feature explanation $\mathbf{r}_u$, we obtain the difference between the predictions for a perturbed node u' using the perturbed and the masked node features, *i.e.,*

$$||\hat{\mathbf{y}}_{u'} - \hat{\mathbf{y}}_{u'}^E||_2 \leq \gamma_{11} \, ||\mathbf{x}_{u'} - (\mathbf{r}_u \circ \mathbf{x}_{u'})||_2,$$

where $\hat{\mathbf{y}}_{u'}$ is the softmax prediction using the perturbed node feature $\mathbf{x}_{u'} = \mathbf{x}_u + \tau$, and as per the definition of faithfulness we use the explanation mask of node u for node u'. Finally, we get:

$$||\hat{\mathbf{y}}_{u'} - \hat{\mathbf{y}}_{u'}^E||_2 \leq \gamma_{11} \, ||(\mathbf{1} - \mathbf{r}_u) \circ \mathbf{x}_{u'}||_2 \tag{25}$$

For faithfulness, we generate a set of $\mathcal{K}$ perturbed nodes and get $|\mathcal{K}|$ predictions from the model for each of the corresponding perturbations. Using Eqns. 23 and 25, and getting the predictions from all $|\mathcal{K}|$ perturbations, we get:

$$\sum_{u' \in \mathcal{K}} ||\hat{\mathbf{y}}_{u'} - \hat{\mathbf{y}}_{u'}^E||_2 \leq \gamma_{11} \, ||(\mathbf{1} - \mathbf{r}_u) \circ \mathbf{x}_u)||_2 + \gamma_{11} \sum_{u' \in \mathcal{K}} ||(\mathbf{1} - \mathbf{r}_u) \circ \mathbf{x}_{u'}||_2$$

$$\leq \gamma_{11} \, ||(\mathbf{1} - \mathbf{r}_u) \circ \mathbf{x}_u)||_2 + \gamma_{11} \, ||(\mathbf{1} - \mathbf{r}_u) \circ \sum_{u' \in \mathcal{K}} \mathbf{x}_{u'}||_2,$$

Assuming τ to be drawn from a normal distribution, we get: $\sum_{u' \in \mathcal{K}} \mathbf{x}_{u'} = |\mathcal{K}|\mathbf{x}_u + \sum_{u' \in \mathcal{K}} \tau_k$. For sufficiently large $|\mathcal{K}|$, we have: $\sum_{u' \in \mathcal{K}} (\mathbf{x}_u')_k \approx |\mathcal{K}|\mathbf{x}_u$. Putting everything together,

$$\sum_{u' \in \mathcal{K}} ||\hat{\mathbf{y}}_{u'} - \hat{\mathbf{y}}_{u'}^E||_2 \leq \gamma_{11} \, ||(\mathbf{1} - \mathbf{r}_u) \circ \mathbf{x}_u)||_2 + \gamma_{11} \, |\mathcal{K}| \, ||(\mathbf{1} - \mathbf{r}_u) \circ \mathbf{x}_u||_2$$

$$\leq \gamma_{11} \, (1 + |\mathcal{K}|) \, ||(\mathbf{1} - \mathbf{r}_u) \circ \mathbf{x}_u||_2$$

For a GNN model with L message-passing layers and one fully-connected layer for node classification, γ_{11} takes the general form of:

$$\gamma_{11} = \mathcal{C}_{\text{fc}} \, ||\mathbf{W}_{\text{fc}}||_2 \prod_{l=1}^{L} \mathcal{C}_l ||\mathbf{W}_a^l||_2, \tag{26}$$

where $\mathcal{C}_{\text{fc}}$ is the Lipschitz constant for the softmax activation operating on the fully-connected layer, $\mathbf{W}_{\text{fc}}$ is the weight matrix associated with the fully-connected layer, $\mathcal{C}_l$ is the Lipschitz constant of the softplus activation of each message-passing layer, and $\mathbf{W}_a^l$ is the self-attention weight associated with the l-th message-passing layer.

Edge explanations. Note, the difference between the predictions for a perturbed node u' using the perturbed and the masked node features will be similar to Eqn. 24 as for faithfulness, the perturbations are made only in node u, *i.e.,*

$$||\hat{\mathbf{y}}_{u'} - \hat{\mathbf{y}}_{u'}^E||_2 \leq \gamma_{12} \, ||\Delta_{\mathbf{x}_v}||_2,$$

Also, since we use the same explanation for all the nodes in set $\mathcal{K}$, the bound for faithfulness using edge explanations is given by:

$$\sum_{u' \in \mathcal{K}} ||\hat{\mathbf{y}}_{u'} - \hat{\mathbf{y}}_{u'}^E||_2 \leq \gamma_{12} \, (1 + |\mathcal{K}|) \, ||\Delta_{\mathbf{x}_v}||_2,$$

where as in Eqn. 26, γ_{12} can take the general form for L message-passing layers as: $\gamma_{12} = \mathcal{C}_{\text{fc}} \, ||\mathbf{W}_{\text{fc}}||_2 \, \prod_{l=1}^{L} \mathcal{C}_l ||\mathbf{W}_n^l||_2$.

B.2 Analyzing Stability of GNN Explanation Methods

B.2.1 Gradient Explanation

Theorem 2. *Given a non-linear activation function σ that is Lipschitz continuous, the stability property (Sec. 3.2, Eqn. 2) of explanation E_u returned by Gradients method can be bounded as follows:*

$$||\nabla_{\mathbf{x}_{u'}} f - \nabla_{\mathbf{x}_u} f||_p \leq \gamma_3 ||\mathbf{x}_{u'} - \mathbf{x}_u||_p, \tag{27}$$

where γ_3 is a constant, $\mathbf{x}_u$ is the original node feature, and $\mathbf{x}_{u'}$ is the perturbed node feature.

Proof. Similar to Sec. B.1, let us consider a two-layer GNN model trained on a node classification task using softmax cross-entropy loss function with the first layer a message-passing GNN layer and the second layer as a fully-connected layer. The cross-entropy (CE) loss is given as:

$$\text{CE} = -\sum_i y_i \log \hat{y}_u, \tag{28}$$

where $\mathbf{y}$ is a vector with one one non-zero element (which is 1), $\hat{\mathbf{y}}_u = \text{softmax}(\mathbf{h}_u^2)$, $\mathbf{h}_u^2 = \mathbf{W}_{\text{fc}} \mathbf{h}_u^1 + \mathbf{b}$, and $\mathbf{h}_u^1 = \text{sp}(\mathbf{W}_a^1 \mathbf{x}_u + \mathbf{W}_n^1 \sum_{v \in \mathcal{N}_u} \mathbf{x}_v)$. $\mathbf{W}_n^1$ is the weight matrix associated with the neighbors of node u and $\mathbf{W}_a^1$ is the self-attention weight matrix at layer one. For the fully-connected layer, we have $\mathbf{W}_{\text{fc}}$ as the weight matrix and $\mathbf{b}$ as the bias term. "sp" is the softplus activation function which is a smooth approximation of the ReLU function. For stability, we generate $\mathbf{x}_{u'}$ by adding noise to the node features of node u and keep everything else constant. Therefore, $\mathbf{h}_{u'}^1 = \text{sp}(\mathbf{W}_a^1 \mathbf{x}_{u'} + \mathbf{W}_n^1 \sum_{v \in \mathcal{N}_u'} \mathbf{x}_v)$. Now, the differentiation of the model *w.r.t.* the node features can be given as:

$$\nabla_{\mathbf{x}_u} f = \frac{\partial(\text{CE})}{\partial \mathbf{x}_u} = \frac{\partial(\text{CE})}{\partial \mathbf{h}_u^2} \frac{\partial \mathbf{h}_u^2}{\partial \mathbf{h}_u^1} \frac{\partial \mathbf{h}_u^1}{\partial \mathbf{x}_u}, \qquad \text{(By chain rule)}$$

Note, the advantage of using *softplus* activation function is that it is differentiable for all x, *i.e.,*

$$\text{sp}(x) = ln(1 + \exp^x)$$
$$\frac{\partial(\text{sp}(x))}{\partial \mathbf{x}} = \frac{\exp^x}{1 + \exp^x} \cdot \frac{(1/\exp^x)}{(1/\exp^x)}$$
$$= \frac{1}{1 + \exp^{-x}}$$
$$= \sigma(x),$$

where $\sigma(\cdot)$ is the sigmoid activation function. Putting it all together we get,

$$\nabla_{\mathbf{x}_u} f = (\mathbf{y}_u - \hat{\mathbf{y}}_u)(\mathbf{W}_{\text{fc}})^T \sigma(\mathbf{W}_a^1 \mathbf{x}_u + \mathbf{W}_n^1 \sum_{v \in \mathcal{N}_u} \mathbf{x}_v)(\mathbf{W}_a^1)^T \tag{29}$$

$$\nabla_{\mathbf{x}_{u'}} f = (\mathbf{y}_u - \hat{\mathbf{y}}_u)(\mathbf{W}_{\text{fc}})^T \sigma(\mathbf{W}_a^1 \mathbf{x}_{u'} + \mathbf{W}_n^1 \sum_{v \in \mathcal{N}_u'} \mathbf{x}_v)(\mathbf{W}_a^1)^T \tag{30}$$

Note, $\hat{\mathbf{y}}_u$ is same for both original and perturbed node according to the Definition 2 in Sec. 3 and we drop the second neighborhood term since the probability (p_r) of rewiring the edges is very small to maintain the original graph structure. Hence, subtracting the explanations (model gradients) for the original and perturbed node features and taking the norm on both sides, we get:

$$||\nabla_{\mathbf{x}_{u'}} f - \nabla_{\mathbf{x}_u} f||_p = ||(\mathbf{y}_u - \hat{\mathbf{y}}_u)(\mathbf{W}_{\text{fc}})^T \big(\sigma(\mathbf{W}_a^1 \mathbf{x}_{u'}) - \sigma(\mathbf{W}_a^1 \mathbf{x}_u)\big)(\mathbf{W}_a^1)^T||_p,$$

Using Cauchy-Schwartz inequality, we get:

$$||\nabla_{\mathbf{x}_{u'}} f - \nabla_{\mathbf{x}_u} f||_p \leq ||\mathbf{y}_u - \hat{\mathbf{y}}_u||_p \, ||(\mathbf{W}_{\text{fc}})^T||_p \, ||\sigma(\mathbf{W}_a^1 \mathbf{x}_{u'}) - \sigma(\mathbf{W}_a^1 \mathbf{x}_u)||_p \, ||(\mathbf{W}_a^1)^T||_p$$

Assuming that $\sigma(\cdot)$ is normalized Lipschitz, *i.e.,* $||\sigma(b) - \sigma(a)||_p \leq ||b - a||_p$, we get,

$$||\nabla_{\mathbf{x}_{u'}} f - \nabla_{\mathbf{x}_u} f||_p \leq ||\mathbf{y}_u - \hat{\mathbf{y}}_u||_p \, ||(\mathbf{W}_{\text{fc}})^T||_p \, ||\mathbf{W}_a^1 \mathbf{x}_{u'} - \mathbf{W}_a^1 \mathbf{x}_u||_p \, ||(\mathbf{W}_a^1)^T||_p$$
$$\leq ||\mathbf{y}_u - \hat{\mathbf{y}}_u||_p \, ||(\mathbf{W}_{\text{fc}})^T||_p \, ||\mathbf{W}_a^1(\mathbf{x}_{u'} - \mathbf{x}_u)||_p \, ||(\mathbf{W}_a^1)^T||_p$$
$$\leq ||\mathbf{y}_u - \hat{\mathbf{y}}_u||_p \, ||(\mathbf{W}_{\text{fc}})^T||_p \, ||\mathbf{W}_a^1||_p \, ||\mathbf{x}_{u'} - \mathbf{x}_u||_p \, ||(\mathbf{W}_a^1)^T||_p$$
$$\text{(Using Cauchy-Schwartz inequality)}$$
$$\leq \gamma_3 \, ||\mathbf{x}_{u'} - \mathbf{x}_u||_p,$$

where $\gamma_3 = ||\mathbf{y}_u - \hat{\mathbf{y}}_u||_p \, ||(\mathbf{W}_{\text{fc}})^T||_p \, ||\mathbf{W}_a^1||_p \, ||(\mathbf{W}_a^1)^T||_p$.

For a GNN model with L message-passing layers and one fully-connected layer for node classification, γ_3 takes the general form of:

$$\gamma_3 = ||\mathbf{y}_u - \hat{\mathbf{y}}_u||_p \, ||(\mathbf{W}_{\text{fc}})^T||_p \prod_{l=1}^{L} ||\mathbf{W}_a^l||_p \, ||(\mathbf{W}_a^1)^T||_p, \tag{31}$$

where $\mathbf{W}_a^l$ is the self-attention weight associated with the l-th message-passing layer.

B.2.2 GraphMASK

Setup. GraphMASK computes the parameters π for the erasure function using fully-connected layers with non-linearity and layer-wise normalization. The scalar location parameter $z_{u,v}^l$ is given as:

$$z_{u,v}^l = \mathbf{W}_2^l \, \text{sp}(\text{LN}^l(\mathbf{W}_1^l \mathbf{q}_{u,v}^l)), \tag{32}$$

where sp is the softplus activation function, LN is the layer normalization function, and $\mathbf{q}_{u,v}^l$ represents the concatenated representations of $\mathbf{h}_u^l$ and $\mathbf{h}_v^l$. Note, the representations at $l=0$ are simply the node features in the original graph $\mathbf{x}_u$ and $\mathbf{x}_v$. Since we are considering the task of node-classification, there is no relation-specific representation with respect to each edge. For explaining node u's prediction, GraphMASK generates $z_{u,v}^l$ for all its incident edges. Finally, the parameters π of the erasure function are trained on multiple datapoints, and then used for explaining predictions [39]. For deriving the instability and counterfactual fairness mismatch of GraphMASK, we first state a lemma that helps us prove that a layer normalization function is Lipschitz.

Lemma 1. *A normalization function LN for layer l is Lipschitz continuous, i.e.,*

$$||\text{LN}^l(\mathbf{h}_{u'}^l) - \text{LN}^l(\mathbf{h}_u^l)||_2 \leq C_{\text{LN}}^l \, ||(\mathbf{h}_{u'}^l - \mathbf{h}_u^l)||_2, \tag{33}$$

where C_{LN}^l is the Lipschitz constant of the normalization function for layer l.

Proof. The layer normalization function is a reparametrization trick that significantly reduces the problem of coordinating updates across different layers. A given representation $\mathbf{h}_u^l$ is normalized using mean and standard deviation parameters that are learned during the training stage, *i.e.,*

$$\text{LN}^l(\mathbf{h}_u^l) = \frac{(\mathbf{h}_u^l - \mu^l)}{\varsigma^l}, \tag{34}$$

where μ^l is the mean and ς^l is the standard deviation of the representations at layer l, and are fixed after the training completes. Using Eqn. 34, the difference between the layer normalized output at layer l of a perturbed and original representation can be given as:

$$\text{LN}^l(\mathbf{h}_{u'}^l) - \text{LN}^l(\mathbf{h}_u^l) = \frac{(\mathbf{h}_{u'}^l - \mu^l)}{\varsigma^l} - \frac{(\mathbf{h}_u^l - \mu^l)}{\varsigma^l}$$

$$\text{LN}^l(\mathbf{h}_{u'}^l) - \text{LN}^l(\mathbf{h}_u^l) = \frac{(\mathbf{h}_{u'}^l - \mathbf{h}_u^l)}{\varsigma^l}$$

Taking L_2-norm on both sides and applying Cauchy-Schwartz inequality, we get:

$$||\text{LN}^l(\mathbf{h}_{u'}^l) - \text{LN}^l(\mathbf{h}_u^l)||_2 \leq ||\frac{1}{\varsigma^l}||_2 \, ||(\mathbf{h}_{u'}^l - \mathbf{h}_u^l)||_2$$

For consistency, we define $C_{\text{LN}}^l = ||\frac{1}{\varsigma^l}||_2$ as the Lipschitz constant for the lth normalization layer.

Theorem 3. *Given concatenated embeddings of node u and v, the stability property (Sec. 3.2, Eqn. 2) of explanation E_u returned by GraphMASK method can be bounded as follows:*

$$||z_{u',v}^l - z_{u,v}^l||_2 \leq \gamma_4^l \, ||\mathbf{q}_{u',v}^l - \mathbf{q}_{u,v}^l||_2, \tag{35}$$

where γ_4^l denotes the Lipschitz constant which is a product of the weights of the l-th fully-connected layer, and the Lipschitz constants for the layer normalization function and softplus activation function.

Proof. Using Eqn. 32, the scalar location parameter for a perturbed node u' can be written as:

$$z_{u',v}^l = \mathbf{W}_2^l \, \text{sp}(\text{LN}^l(\mathbf{W}_1^l \mathbf{q}_{u',v}^l))$$

Note, for explanation all the parameters of the fully-connected layers are fixed as they are trained initially using a set of training data points.

$$z_{u',v}^l - z_{u,v}^l = \mathbf{W}_2^l \, \text{sp}(\text{LN}^l(\mathbf{W}_1^l \mathbf{q}_{u',v}^l)) - \mathbf{W}_2^l \, \text{sp}(\text{LN}^l(\mathbf{W}_1^l \mathbf{q}_{u,v}^l))$$

$$z_{u',v}^l - z_{u,v}^l = \mathbf{W}_2^l \left(\text{sp}(\text{LN}^l(\mathbf{W}_1^l \mathbf{q}_{u',v}^l)) - \text{sp}(\text{LN}^l(\mathbf{W}_1^l \mathbf{q}_{u,v}^l)) \right)$$

Taking L_2-norm on both sides and applying Cauchy-Schwartz inequality, we get:

$$||z_{u',v}^l - z_{u,v}^l||_2 \leq ||\mathbf{W}_2^l||_2 \, ||\text{sp}(\text{LN}^l(\mathbf{W}_1^l \mathbf{q}_{u',v}^l)) - \text{sp}(\text{LN}^l(\mathbf{W}_1^l \mathbf{q}_{u,v}^l))||_2$$

$$\leq C_{\text{SP}}||\mathbf{W}_2^l||_2 \, ||\text{LN}^l(\mathbf{W}_1^l \mathbf{q}_{u',v}^l) - \text{LN}^l(\mathbf{W}_1^l \mathbf{q}_{u,v}^l)||_2, \qquad \text{(Using Corollary 1)}$$

where C_{SP} is the Lipschitz constant for the softplus activation function. Simplifying further we get:

$$||z_{u',v}^l - z_{u,v}^l||_2 \leq C_{\text{SP}} \, C_{\text{LN}}^l ||\mathbf{W}_2^l||_2 \, ||\mathbf{W}_1^l \mathbf{q}_{u',v}^l - \mathbf{W}_1^l \mathbf{q}_{u,v}^l||_2 \qquad \text{(Using Lemma 1)}$$

$$\leq C_{\text{SP}} \, C_{\text{LN}}^l ||\mathbf{W}_2^l||_2 \, ||\mathbf{W}_1^l||_2 \, ||\mathbf{q}_{u',v}^l - \mathbf{q}_{u,v}^l||_2 \qquad \text{(Using Cauchy-Schwartz inequality)}$$

Hence, for a given layer l the difference between the scalar location parameter of a perturbed and original node u is given by:

$$||z_{u',v}^l - z_{u,v}^l||_2 \leq \gamma_4^l \, ||\mathbf{q}_{u',v}^l - \mathbf{q}_{u,v}^l||_2, \tag{36}$$

where $\gamma_4^l = C_{\text{SP}} \, C_{\text{LN}}^l ||\mathbf{W}_2^l||_2 \, ||\mathbf{W}_1^l||_2$. Now, for explaining the prediction for node u, we can repeat this process for all edges $(u, v) \in \mathcal{E}$ in the neighborhood $\mathcal{N}_u$ of node u and generate the matrix $\mathbf{Z}^l$. It is to be noted, that the values of the $z_{u,v}^l$ elements represent whether a given edge can be dropped or not—an explanation. Further, the composition of multiple Lipschitz continuous functions with Lipschitz constants $\{\mathcal{L}_1, \ldots, \mathcal{L}_L\}$ is a new Lipschitz continuous function with $\mathcal{L}_1 \times \cdots \times \mathcal{L}_L$ as the Lipschitz constant [11]. Using the formulation for a single layer l (Eqn. 36), we can generate a bound for all L layers of the model f, where the Lipschitz constant will be: $\prod_{l=1}^L \gamma_4^l$.

B.2.3 GraphLIME

Setup. We use Gaussian kernel for both input and the predictions of all neighbors of node u.

$$K(x_i^{(k)}, x_j^{(k)}) = \exp\big(-\frac{(x_i^{(k)} - x_j^{(k)})^2}{2\sigma_x^2}\big); L(y_i^{(k)}, y_j^{(k)}) = \exp\big(-\frac{||y_i^{(k)} - y_j^{(k)}||_2^2}{2\sigma_y^2}\big), \quad (37)$$

The HSIC Lasso objective can be regarded as a minimum redundancy maximum relevancy (mRMR) based feature selection method [32]. Eqn. 14 can be rewritten as:

$$||\mathbf{L} - \sum_{k=1}^{M} \beta_k \mathbf{K}^{(k)}||_F^2 = \text{HSIC}(\mathbf{y}, \mathbf{y}) + \sum_{i=1}^{M} \beta_i \text{HSIC}(\mathbf{x}_i, \mathbf{y}) + \sum_{i,j=1}^{M} \beta_i \beta_j \text{HSIC}(\mathbf{x}_i, \mathbf{x}_j), \quad (38)$$

where $\text{HSIC}(\mathbf{x}_i, \mathbf{y}) = \text{tr}(\mathbf{K}^{(k)}, \mathbf{L})$ is a kernel-based independence measure called the (empirical) Hilbert-Schmidt independence criterion (HSIC) [12]. Further, the HSIC lasso is a convex optimization problem [49] and hence given a set of features it will learn feature importance that fit to the predicted labels. We now derive the upper bound for the explanation generated by GraphLIME (or simply GLIME) for the k-th node feature. We exclude the sparsity regularizer in our analysis as GLIME enforces sparsity by selecting the top-P features after the optimization.

Theorem 4. *Given the centered Gram matrices for the original and perturbed node attributes, the stability property (Sec. 3.2, Eqn. 2) of explanation E_u returned by GraphLIME method can be bounded as follows:*

$$||\beta_k' - \beta_k||_F \leq \gamma_2 \cdot \text{tr}((\frac{1}{\mathbf{e}^T \mathbf{W}^{-1} \mathbf{e}})^{-1} - \mathbf{I}), \quad (39)$$

where β_k' and β_k are the feature importance generated by GraphLIME for the original and perturbed node features, γ_2 is a constant independent of the added noise, $\mathbf{e}$ is a vector of all ones, and $\mathbf{W}$ is a matrix comprising of the added noise terms.

Proof. Note, $||Q||_F^2 = \text{tr}(QQ^T) = \text{tr}(QQ)$, where Q is a symmetric matrix and $\text{tr}(\cdot)$ is the trace of the matrix. Using this, the objective function can be simplified as:

$$\frac{1}{2}||\mathbf{L} - \sum_{i=1}^{M} \beta_i \mathbf{K}^{(i)}||_F^2$$

$$= \frac{1}{2}\text{tr}\big((\mathbf{L} - \sum_{i=1}^{M} \beta_i \mathbf{K}^{(i)}) \cdot (\mathbf{L}^T - \sum_{i=1}^{M} \beta_i \mathbf{K}^{(i)^T})\big)$$

$$= \frac{1}{2}\text{tr}\big((\mathbf{L} - \sum_{i=1}^{M} \beta_i \mathbf{K}^{(i)}) \cdot (\mathbf{L}^T - \sum_{i=1}^{M} \beta_i \mathbf{K}^{(i)})\big)$$

$$= \frac{1}{2}\text{tr}\big(\mathbf{L}\mathbf{L}^T - 2\sum_{i=1}^{M} \beta_i \mathbf{L}\mathbf{K}^{(i)} + \sum_{i,j=1}^{M} \beta_i \beta_j \mathbf{K}^{(i)}\mathbf{K}^{(j)}\big)$$

We want to minimize the above objective function O. We take the partial derivative of O w.r.t. β_k:

$$\frac{\partial O}{\partial \beta_k} = -\mathbf{L}\mathbf{K}^{(k)} + \sum_{j=1}^{M} \beta_j \mathbf{K}^{(j)}\mathbf{K}^{(k)} = 0$$

$$\implies -\mathbf{L}\mathbf{K}^{(k)} + \sum_{j=1}^{M} \beta_j \mathbf{K}^{(j)}\mathbf{K}^{(k)} = 0$$

$$\implies (-\mathbf{L} + \sum_{j=1}^{M} \beta_j \mathbf{K}^{(j)})\mathbf{K}^{(k)} = 0$$

$$\implies (-\mathbf{L} + \sum_{j=1;j\neq k}^{M} \beta_j \mathbf{K}^{(j)} + \beta_k \mathbf{K}^{(k)})\mathbf{K}^{(k)} = 0$$

We finally get,

$$\beta_k \mathbf{K}^{(k)} = \mathbf{L} - \sum_{j=1; j \neq k}^{M} \beta_j \mathbf{K}^{(j)} \tag{40}$$

The gram matrix is invertible as it is a full rank symmetric matrix with all the diagonal elements as 1 (since $K(x_i, x_i) = 1$) and so:

$$\beta_k = \bar{\mathbf{L}}(\mathbf{K}^{(k)})^{-1}, \tag{41}$$

where $\bar{\mathbf{L}} = \mathbf{L} - \sum_{j=1; j \neq k}^{M} \beta_j \mathbf{K}^{(j)}$.

On adding infinitesimal noise η to the k-th feature, we obtain a new gram matrix given by: $\mathbf{K}^{(k)'} = \mathbf{K}^{(k)} \circ \mathbf{W}$, where $\mathbf{W} \in \mathbb{R}^{M \times M}$ is a function of η and x_i. For instance, adding noise η to $x_i^{(k)}$, we get $K'(x_i^{(k)}, x_j^{(k)})$ as:

$$K'(x_i^{(k)}, x_j^{(k)}) = \exp\left(-\frac{(x_i^{(k)} + \eta - x_j^{(k)})^2}{2\sigma_x^2}\right)$$

$$= \exp\left(-\frac{(x_i^{(k)} - x_j^{(k)})^2 + \eta^2 + 2\eta(x_i^{(k)} - x_j^{(k)})}{2\sigma_x^2}\right)$$

$$= \exp\left(-\frac{(x_i^{(k)} - x_j^{(k)})^2 + 2\eta(x_i^{(k)} - x_j^{(k)})}{2\sigma_x^2}\right) \qquad (\eta^2 = 0 \text{ as } \eta \text{ is infinitesimal noise})$$

$$= \exp\left(-\frac{(x_i^{(k)} - x_j^{(k)})^2}{2\sigma_x^2}\right) \cdot \exp\left(-\frac{2\eta(x_i^{(k)} - x_j^{(k)})}{2\sigma_x^2}\right)$$

The importance for the k-th node feature is generated by GraphLIME as β_k. We can now represent the Frobenius norm of the difference between the explanations from GLIME for the original and noisy graph as:

$$||\beta_k' - \beta_k||_F = ||\bar{\mathbf{L}}(\mathbf{K}^{(k)'})^{-1} - \bar{\mathbf{L}}(\mathbf{K}^{(k)})^{-1}||_F$$

$$= ||\bar{\mathbf{L}}\left((\mathbf{K}^{(k)'})^{-1} - (\mathbf{K}^{(k)})^{-1}\right)||_F$$

$$\leq ||\bar{\mathbf{L}}||_F \, ||(\mathbf{K}^{(k)'})^{-1} - (\mathbf{K}^{(k)})^{-1}||_F \qquad \text{(Using Cauchy-Schwartz inequality)}$$

$$\leq ||\bar{\mathbf{L}}||_F \, ||(\mathbf{K}^{(k)} \circ \mathbf{W})^{-1} - (\mathbf{K}^{(k)})^{-1}||_F$$

$$\leq ||\bar{\mathbf{L}}||_F \, ||(\frac{1}{\mathbf{e}^T \mathbf{W}^{-1} \mathbf{e}} \mathbf{K}^{(k)})^{-1} - (\mathbf{K}^{(k)})^{-1}||_F, \qquad \text{(Using Theorem 3.1 from [35])}$$

where $\mathbf{e}$ is a $m \times 1$ vector of all ones. Note, for using Theorem 3.1 from [35] we need: 1) $\mathbf{K}^{(k)}$ is positive semidefinite; and 2) $\mathbf{W}$ is positive definite or is almost positive definite and invertible. (1) is true by definition as $\mathbf{K}^{(k)}$ is a gram matrix and they are positive semidefinite. For (2), let us consider a case where $\mathbf{W} \in \mathbb{R}^{2 \times 2}$. Using the Gaussian kernel $\mathbf{K}^{(k)}$, the perturbed gram matrix $\mathbf{K}^{(k)'}$ is:

$$\mathbf{K}^{(k)'} = \begin{bmatrix} 1 & \exp\left(-\frac{(x_1^{(k)} - x_2^{(k)})^2}{2\sigma_x^2}\right) \cdot \exp\left(-\frac{2\eta(x_1^{(k)} - x_2^{(k)})}{2\sigma_x^2}\right) \\ \exp\left(-\frac{(x_1^{(k)} - x_2^{(k)})^2}{2\sigma_x^2}\right) \cdot \exp\left(-\frac{2\eta(x_1^{(k)} - x_2^{(k)})}{2\sigma_x^2}\right) & 1 \end{bmatrix}$$

$$= \begin{bmatrix} 1 & \exp\left(-\frac{(x_1^{(k)} - x_2^{(k)})^2}{2\sigma_x^2}\right) \\ \exp\left(-\frac{(x_1^{(k)} - x_2^{(k)})^2}{2\sigma_x^2}\right) & 1 \end{bmatrix} \circ \begin{bmatrix} 1 & \exp\left(-\frac{2\eta(x_1^{(k)} - x_2^{(k)})}{2\sigma_x^2}\right) \\ \exp\left(-\frac{2\eta(x_1^{(k)} - x_2^{(k)})}{2\sigma_x^2}\right) & 1 \end{bmatrix}$$

Hence, $\mathbf{W}$ is:

$$\mathbf{W} = \begin{bmatrix} 1 & \exp\left(-\frac{2\eta(x_1^{(k)} - x_2^{(k)})}{2\sigma_x^2}\right) \\ \exp\left(-\frac{2\eta(x_1^{(k)} - x_2^{(k)})}{2\sigma_x^2}\right) & 1 \end{bmatrix} \tag{42}$$

21

For positive definite, we need to show $b^T\mathbf{W}b > 0$ for any non-zero vector b. All the elements of $\mathbf{W}$ are positive and using a b vector with all ones will result in $b^T\mathbf{W}b > 0$. Hence, $\mathbf{W}$ is positive definite. Now, both $\mathbf{W}$ and $\mathbf{K}^{(k)}$ are invertible matrix so we can use the property $(AB)^{-1} = B^{-1}A^{-1}$. Putting everything together we get:

$$||\beta'_k - \beta_k||_F \leq ||\bar{\mathbf{L}}||_F \, ||(\mathbf{K}^{(k)})^{-1}(\frac{1}{\mathbf{e}^T\mathbf{W}^{-1}\mathbf{e}})^{-1} - (\mathbf{K}^{(k)})^{-1}||_F$$

$$\leq ||\bar{\mathbf{L}}||_F \, ||(\mathbf{K}^{(k)})^{-1}\big((\frac{1}{\mathbf{e}^T\mathbf{W}^{-1}\mathbf{e}})^{-1} - \mathbf{I}\big)||_F$$

$$\leq ||\bar{\mathbf{L}}||_F \, ||(\mathbf{K}^{(k)})^{-1}||_F \, ||(\frac{1}{\mathbf{e}^T\mathbf{W}^{-1}\mathbf{e}})^{-1} - \mathbf{I}||_F \qquad \text{(Using Cauchy-Schwartz inequality)}$$

$$\leq \text{tr}(\bar{\mathbf{L}}) \, \text{tr}((\mathbf{K}^{(k)})^{-1}) \, \text{tr}((\frac{1}{\mathbf{e}^T\mathbf{W}^{-1}\mathbf{e}})^{-1} - \mathbf{I})$$

$$\leq \gamma_2 \, \cdot \, \text{tr}((\frac{1}{\mathbf{e}^T\mathbf{W}^{-1}\mathbf{e}})^{-1} - \mathbf{I}),$$

where $\gamma_2 = \text{tr}(\bar{\mathbf{L}}) \, \text{tr}((\mathbf{K}^{(k)})^{-1})$ is a constant independent of the added noise.

B.3 Analyzing Fairness of GNN Explanation Methods

Theorem 5. *Given a node u, a sensitive attribute s, and a set $\mathcal{K}$ comprising of node u and its perturbations, the group fairness property (Sec. 3.3, Eqn. 4) of an explanation E_u corresponding to node u can be bounded as follows:*

$$| \, \text{SP}(\hat{\mathbf{y}}_{\mathcal{K}}) - \text{SP}(\hat{\mathbf{y}}_{\mathcal{K}}^{E_u}) \, | \leq \sum_{s\in\{0,1\}} |\text{Err}_{D_s}(f(t(E_u,\mathcal{G}_{u'})) - f(\mathcal{G}_{u'}))|, \qquad (43)$$

where $\text{SP}(\hat{\mathbf{y}}_{\mathcal{K}})$ and $\text{SP}(\hat{\mathbf{y}}_{\mathcal{K}}^{E_u})$ are statistical parity estimates as defined in Sec. 3.3, D is the joint distribution over the node attributes $\mathbf{x}_{u'}$ in graph $\mathcal{G}_{u'}$ and their respective labels $\mathbf{y}_{u'}$ for all nodes $u' \in \mathcal{K}$, D_s is the conditional distribution of D given a particular value of the sensitive attribute s, and $\text{Err}_D(\cdot) = \mathbb{E}_D[\mathbf{y}_{u'} - f(\mathcal{G}_{u'})]$ is the error of the model f under the joint distribution D.

Proof. For group fairness, we define the total variation divergence d_{TV} to measure the difference between two probability distributions, *i.e.,* $\hat{\mathbf{y}}_{\mathcal{K}}$ and $\hat{\mathbf{y}}_{\mathcal{K}}^{E_u}$. For a given binary sensitive attribute $s \in \{0, 1\}$, we can write: $d_{\text{TV}}(D_s(\mathbf{y}_{u'}), D_s(\hat{\mathbf{y}}_{\mathcal{K}})) \leq \mathbb{E}_{D_s}[|\mathbf{y}_{u'} - f(\mathcal{G}_{u'})|]$ [53]. The total variation divergence is symmetrical and satisfies triangle inequality. Hence, we have:

$$d_{\text{TV}}(D_0(\mathbf{y}_{u'}), D_1(\mathbf{y}_{u'})) \leq d_{\text{TV}}(D_0(\mathbf{y}_{u'}), D_0(\hat{\mathbf{y}}_{\mathcal{K}})) + d_{\text{TV}}(D_0(\hat{\mathbf{y}}_{\mathcal{K}}), D_1(\hat{\mathbf{y}}_{\mathcal{K}})) + $$
$$d_{\text{TV}}(D_1(\mathbf{y}_{u'}), D_1(\hat{\mathbf{y}}_{\mathcal{K}}))$$

Now, the middle term in the right side of the inequality is the statistical parity (SP) for the binary sensitive attribute and therefore we can simplify the equation as:

$$d_{\text{TV}}(D_0(\mathbf{y}_{u'}), D_1(\mathbf{y}_{u'})) \leq d_{\text{TV}}(D_0(\mathbf{y}_{u'}), D_0(\hat{\mathbf{y}}_{\mathcal{K}})) + \text{SP}(\hat{\mathbf{y}}_{\mathcal{K}}) + d_{\text{TV}}(D_1(\mathbf{y}_{u'}), D_1(\hat{\mathbf{y}}_{\mathcal{K}})) \qquad (44)$$

Similarly, using the explanation E, we can write a similar inequality of the group predictions $\hat{\mathbf{y}}_{\mathcal{K}}^{E_u}$ and equate the left hand side terms to get:

$$d_{\text{TV}}(D_0(\mathbf{y}_{u'}), D_0(\hat{\mathbf{y}}_{\mathcal{K}})) + \text{SP}(\hat{\mathbf{y}}_{\mathcal{K}}) + d_{\text{TV}}(D_1(\mathbf{y}_{u'}), D_1(\hat{\mathbf{y}}_{\mathcal{K}})) = $$
$$d_{\text{TV}}(D_0(\mathbf{y}_{u'}), D_0(\hat{\mathbf{y}}_{\mathcal{K}}^{E_u})) + \text{SP}(\hat{\mathbf{y}}_{\mathcal{K}}^{E_u}) + d_{\text{TV}}(D_1(\mathbf{y}_{u'}), D_1(\hat{\mathbf{y}}_{\mathcal{K}}^{E_u})) \qquad (45)$$

Using Lemma 3.1 of [53], we can write $d_{\text{TV}}(D_s(\mathbf{y}_{u'}), D_s(\hat{\mathbf{y}}_{\mathcal{K}})) \leq \text{Err}_{D_s}(f(\mathcal{G}_{u'}))$. Further simplification of Eqn. 45 and plugging the lemma, we get:
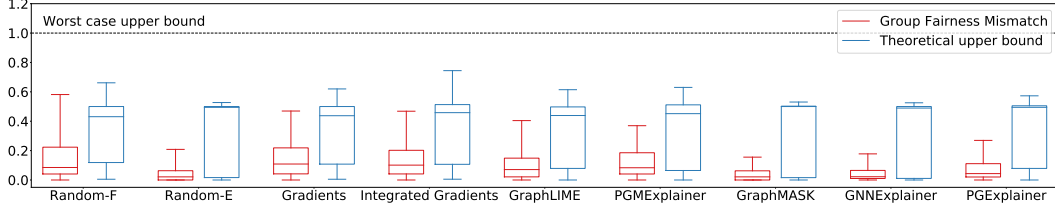
Figure 2: The empirically calculated group fairness mismatch measure (in red) and our theoretical upper bounds for group fairness mismatch (in blue) for nine explanation methods. Results show that no explanation method violate the group fairness bounds for the German credit graph dataset.

$$\text{SP}(\hat{\mathbf{y}}_{\mathcal{K}}^{E_u}) - \text{SP}(\hat{\mathbf{y}}_{\mathcal{K}}) = d_{\text{TV}}(D_0(\mathbf{y}_{u'}), D_0(\hat{\mathbf{y}}_{\mathcal{K}}^{E_u})) - d_{\text{TV}}(D_0(\mathbf{y}_{u'}), D_0(\hat{\mathbf{y}}_{\mathcal{K}}))$$
$$+ d_{\text{TV}}(D_1(\mathbf{y}_{u'}), D_1(\hat{\mathbf{y}}_{\mathcal{K}}^{E_u})) - d_{\text{TV}}(D_1(\mathbf{y}_{u'}), D_1(\hat{\mathbf{y}}_{\mathcal{K}})) \tag{46}$$

$$\text{SP}(\hat{\mathbf{y}}_{\mathcal{K}}^{E_u}) - \text{SP}(\hat{\mathbf{y}}_{\mathcal{K}}) \leq \text{Err}_{D_0}(f(t(E_u, \mathcal{G}_{u'}))) - \text{Err}_{D_0}(f(\mathcal{G}_{u'})) + \text{Err}_{D_1}(f(t(E_u, \mathcal{G}_{u'}))) - \text{Err}_{D_1}(f(\mathcal{G}_{u'})) \tag{47}$$

$$\text{SP}(\hat{\mathbf{y}}_{\mathcal{K}}^{E_u}) - \text{SP}(\hat{\mathbf{y}}_{\mathcal{K}}) \leq \text{Err}_{D_0}(f(t(E_u, \mathcal{G}_{u'})) - f(\mathcal{G}_{u'})) + \text{Err}_{D_1}(f(t(E_u, \mathcal{G}_{u'})) - f(\mathcal{G}_{u'})) \tag{48}$$

Taking the absolute value as norms on both sides, we get:

$$|\text{SP}(\hat{\mathbf{y}}_{\mathcal{K}}^{E_u}) - \text{SP}(\hat{\mathbf{y}}_{\mathcal{K}})| \leq |\text{Err}_{D_0}(f(t(E_u, \mathcal{G}_{u'})) - f(\mathcal{G}_{u'})) + \text{Err}_{D_1}(f(t(E_u, \mathcal{G}_{u'})) - f(\mathcal{G}_{u'}))|$$

$$|\text{SP}(\hat{\mathbf{y}}_{\mathcal{K}}^{E_u}) - \text{SP}(\hat{\mathbf{y}}_{\mathcal{K}})| \leq |\text{Err}_{D_0}(f(t(E_u, \mathcal{G}_{u'})) - f(\mathcal{G}_{u'}))| + |\text{Err}_{D_1}(f(t(E_u, \mathcal{G}_{u'})) - f(\mathcal{G}_{u'}))|$$
$$\text{(Using triangle inequality)}$$

$$|\text{SP}(\hat{\mathbf{y}}_{\mathcal{K}}) - \text{SP}(\hat{\mathbf{y}}_{\mathcal{K}}^{E_u})| \leq \sum_{s \in \{0,1\}} |\text{Err}_{D_s}(f(t(E_u, \mathcal{G}_{u'})) - f(\mathcal{G}_{u'}))|.$$

C Experiments

Datasets. The training and testing splits for the *German credit graph*, *Recidivism graph*, and *Credit defaulter graph* dataset is setup following the codes released by [2]. For the *Ogbn-arxiv* citation graph, we use the training and testing data loader[2] provided by [16]. All datasets used in this work are publicly available and are accordingly cited.

Implementation details. For all datasets, we use a mutli-layer GraphSAGE model as our GNN predictor f. For the *German credit graph*, *Recidivism graph*, and *Credit defaulter graph* datasets, we follow [2] and design a model comprising of two GraphSAGE convolution layers with ReLU non-linear activation function and a fully-connected linear classification layer with Softmax activations. The hidden dimensionality of the layers is set to 16.

For the *Ogbn-arxiv* datasets, we follow [16] and design a model comprising of three GraphSAGE convolution layers with ReLU non-linear activation function and a fully-connected linear classification layer with Softmax activations. The hidden dimensionality of the layers is set to 256.

Compute details. We use a Intel(R) Xeon(R) CPU E5-2680 with 250Gb RAM and a single NVIDIA Tesla M40 GPU for all our experiments.

Hyperparameters. For all experiments, we use normal Gaussian noise $\mathcal{N}(0, 1)$ for perturbing node attributes and set the probability of perturbing an attribute dimension to 0.1. For training GraphSAGE, we use an Adam optimizer with a learning rate of 1×10^{-3}, weight decay of 1×10^{-5}, and the number of epochs to 1000. For the GNN explanation methods, all hyperparameters are set following the authors' guidelines.

Now, we discuss the empirical and theoretical bounds for stability, counterfactual fairness, and group fairness of GNN explanation methods.

---

[2] https://ogb.stanford.edu/docs/home/

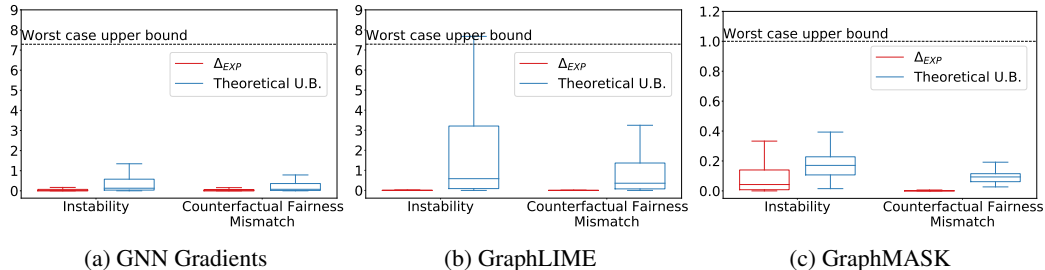(a) GNN Gradients   (b) GraphLIME   (c) GraphMASK

Figure 3: The theoretical upper bounds (in blue) for the instability and counterfactual fairness mismatch metric for (a) GNN Gradients, (b) GraphLIME, and (c) GraphMASK explanation method. Results across both properties show that the empirically calculated explanation differences Δ_{EXP} (in red) do not violate our theoretical bounds when evaluated on the German credit graph dataset.

C.1 Results

Q1) Explanation methods satisfy theoretical bounds across all properties. Fig. 2 shows empirical values and theoretical bounds for group fairness, indicating that no violations of bounds were detected in our experiments. We observe consistent trend between empirically computed group fairness mismatch and theoretical bounds for all nine explanation methods, with the empirical values always lower than our theoretical upper bounds.

In Fig. 3, we show the empirical and theoretical comparison of the bounds for stability and counterfactual fairness for the three representative explanation methods, *viz.* GNN Gradients (Fig. 3a, GraphLIME (Fig. 3b), and GraphMASK (Fig. 3c). Across all explanation methods, the theoretical bounds are well below the worst case upper bound with only some outlier points for stability in GraphLIME. Despite some outlier data points obtaining high theoretical bounds, the median (horizontal line inside each box in Fig. 3) of the theoretical bounds are an order of magnitude smaller than that provided by the worst case upper bound.

Q2) Surrogate model based methods generate most reliable explanations. Results in Table 2 across four datasets show that surrogate model based explanation methods tend to produce more reliable explanations than gradient and perturbation based methods. Specifically, all nine explanation methods are highly unstable across four datasets suggesting the need for explanation methods that are stable to infinitesimally small noise perturbations.

Table 2: Systematic evaluation of GNN explanation methods (random strategies (in grey), gradient methods (in yellow), surrogate methods (in purple), and perturbation methods (in red)). Shown are average values of metrics and standard errors across all nodes in the test set. Arrows (↓) indicate the direction of better performance. Note that fairness does not apply to the ogbn-arxiv dataset (*i.e.,* N/A) as the dataset does not contain sensitive attributes.

| Dataset | Method | Evaluation metrics | | | |
| | | Unfaithfulness (↓) | Instability (↓) | Fairness Mismatch (↓) | |
				Counterfactual	Group
German credit graph	Random Node Attributes	0.208 ± 0.011	0.386 ± 0.006	0.387 ± 0.006	0.165 ± 0.015
	Random Edges	0.049 ± 0.004	0.375 ± 0.001	0.375 ± 0.001	0.061 ± 0.009
	Gradients	0.185 ± 0.010	0.222 ± 0.010	0.137 ± 0.007	0.154 ± 0.012
	Integrated Gradients	0.199 ± 0.011	0.254 ± 0.019	0.210 ± 0.018	0.150 ± 0.012
	GraphLIME	0.158 ± 0.009	0.096 ± 0.013	0.063 ± 0.008	0.114 ± 0.010
	PGMExplainer	0.131 ± 0.007	0.183 ± 0.006	0.185 ± 0.006	0.129 ± 0.010
	GraphMASK	0.034 ± 0.003	0.270 ± 0.008	0.006 ± 0.001	0.046 ± 0.006
	GNNExplainer	0.046 ± 0.004	0.377 ± 0.001	0.359 ± 0.002	0.060 ± 0.009
	PGExplainer	0.074 ± 0.006	0.367 ± 0.004	0.360 ± 0.009	0.079 ± 0.001
Recidivism graph	Random Node Attributes	0.312 ± 0.004	0.403 ± 0.002	0.403 ± 0.002	0.144 ± 0.003
	Random Edges	0.040 ± 0.001	0.376 ± 0.000	0.376 ± 0.000	0.046 ± 0.001
	Gradients	0.233 ± 0.004	0.285 ± 0.003	0.173 ± 0.002	0.114 ± 0.002
	Integrated Gradients	0.308 ± 0.005	0.226 ± 0.003	0.104 ± 0.003	0.139 ± 0.003
	GraphLIME	0.191 ± 0.004	0.264 ± 0.004	0.072 ± 0.003	0.107 ± 0.003
	PGMExplainer	0.128 ± 0.001	0.226 ± 0.002	0.223 ± 0.002	0.130 ± 0.002
	GraphMASK	0.053 ± 0.002	0.251 ± 0.003	0.013 ± 0.000	0.060 ± 0.002
	GNNExplainer	0.042 ± 0.001	0.374 ± 0.000	0.364 ± 0.001	0.051 ± 0.002
	PGExplainer	0.056 ± 0.001	0.371 ± 0.001	0.355 ± 0.002	0.064 ± 0.002
Credit defaulter graph	Random Node Attributes	0.098 ± 0.002	0.426 ± 0.002	0.424 ± 0.002	0.045 ± 0.002
	Random Edges	0.020 ± 0.001	0.376 ± 0.000	0.376 ± 0.000	0.017 ± 0.001
	Gradients	0.092 ± 0.002	0.333 ± 0.002	0.171 ± 0.002	0.042 ± 0.002
	Integrated Gradients	0.147 ± 0.003	0.140 ± 0.002	0.069 ± 0.001	0.053 ± 0.002
	GraphLIME	0.038 ± 0.002	0.225 ± 0.004	0.063 ± 0.003	0.018 ± 0.001
	PGMExplainer	0.283 ± 0.002	0.156 ± 0.002	0.154 ± 0.002	0.161 ± 0.003
	GraphMASK	0.012 ± 0.001	0.036 ± 0.002	0.004 ± 0.000	0.010 ± 0.001
	GNNExplainer	0.021 ± 0.001	0.375 ± 0.000	0.366 ± 0.000	0.019 ± 0.001
	PGExplainer	0.028 ± 0.001	0.364 ± 0.001	0.348 ± 0.002	0.022 ± 0.001
Ogbn-arxiv	Random Node Attributes	0.529 ± 0.002	0.375 ± 0.000	N/A	N/A
	Random Edges	0.431 ± 0.002	0.378 ± 0.001	N/A	N/A
	Gradients	0.528 ± 0.002	0.359 ± 0.001	N/A	N/A
	Integrated Gradients	0.528 ± 0.002	0.372 ± 0.000	N/A	N/A
	GraphLIME	0.260 ± 0.003	0.374 ± 0.004	N/A	N/A
	PGMExplainer	0.413 ± 0.002	0.270 ± 0.002	N/A	N/A
	GraphMASK	0.586 ± 0.001	0.125 ± 0.002	N/A	N/A
	GNNExplainer	0.430 ± 0.002	0.376 ± 0.001	N/A	N/A
	PGExplainer	0.338 ± 0.002	0.381 ± 0.001	N/A	N/A